

RESEARCH

Open Access



Solidified reverse micellar solution-based chitosan-coated solid lipid nanoparticles as a new approach to enhance oral delivery of artemether in malaria treatment

Franklin Chimaobi Kenechukwu^{1*}, Kingsley Chinazam Ugwu¹, Chibuzor Stanley Offorbuike¹, Enyi Moses Ojukwu¹, Thaddeus Harrison Gugu², Reuben Ejike Eze¹, Chinazom Precious Agbo¹, Mumuni Audu Momoh¹, Anthony Ikechukwu Onah³, Chinekwa Sherridan Nwagwu¹, Onyinyechi Lydia Ugorji⁴, Emmanuel Chekwube Ossai⁵, Calister Elochukwu Ugwu⁴, Paul Achile Akpa¹, Aadaeze Chidiebere Echezona¹, Samuel WisdomofGod Uzundu^{1,6}, Chimaobi Odinaka Ugorji⁷, Wilfred Ikechukwu Ugwuoke⁸, Teerapol Srirachana⁹ and Anthony Amaechi Attama¹

Abstract

Solidified reverse micellar technology and surface-modification are promising techniques for improving the biopharmaceutical properties of poorly water-soluble drugs such as artemether, a first-line antimalarial drug. Thus, the aim of this study was to develop and evaluate artemether-loaded chitosan-coated solid lipid nanoparticles (SLNs) based on solidified reverse micellar solution (SRMS) for improved oral malaria therapy. Artemether-loaded and unloaded SLNs were prepared from optimized SRMS (consisting of Phospholipon® 90G and Compritol® ATO 888 at 3:7 ratio) with or without chitosan by high-shear melt-homogenization, and thereafter characterized for physicochemical performance, stability, safety and antimalarial activity using *Plasmodium berghei*-infected mice. Results showed both smooth and irregular particles with a layer of polymer coating in chitosan-modified SLNs, increased drug amorphization as well as compatibility of the drug and excipients employed in the formulations. The optimized formulation was stable and nanomeric (size 292.90 ± 5.01 nm, polydispersity index 0.191 ± 0.09 , and zeta-potential $+32.50 \pm 1.58$ mV) with good encapsulation efficiency (82.03%), demonstrated minimal toxicity on Caco-2 cells, exhibited controlled drug release compared with fast release of artemether suspension and gave significantly ($p < 0.05$) greater antimalarial activity than artemether suspension. Artemether-loaded chitosan-coated SRMS-based SLNs improved the antimalarial activity of the drug and can be pursued as a novel alternative for improved oral malaria treatment.

Keywords Solidified reverse micellar solution, Antimalarial activity, Chitosan, Solid lipid nanoparticles, Artemether, *Plasmodium berghei*

*Correspondence:

Franklin Chimaobi Kenechukwu
chimafrankduff@yahoo.com; frankline.kenechukwu@unn.edu.ng
Full list of author information is available at the end of the article



© The Author(s) 2025. **Open Access** This article is licensed under a Creative Commons Attribution-NonCommercial-NoDerivatives 4.0 International License, which permits any non-commercial use, sharing, distribution and reproduction in any medium or format, as long as you give appropriate credit to the original author(s) and the source, provide a link to the Creative Commons licence, and indicate if you modified the licensed material. You do not have permission under this licence to share adapted material derived from this article or parts of it. The images or other third party material in this article are included in the article's Creative Commons licence, unless indicated otherwise in a credit line to the material. If material is not included in the article's Creative Commons licence and your intended use is not permitted by statutory regulation or exceeds the permitted use, you will need to obtain permission directly from the copyright holder. To view a copy of this licence, visit <http://creativecommons.org/licenses/by-nc-nd/4.0/>.

Introduction

Malaria, a life-threatening disease caused by *Plasmodium* parasites and spread via infected Anopheles mosquitoes, poses a significant global health threat [1]. In many parts of the world, it remains a serious health risk, especially in sub-Saharan Africa, where the disease burden remains as high as 90% [2]. In 2022, there were an estimated 249 million cases and 608,000 deaths worldwide resulting from malaria, with the World Health Organization (WHO) African Region bearing the highest burden [3]. Children under 5 accounted for about 80% of all malaria deaths in Africa. Symptoms range from mild to severe, including fever, chills, headache, fatigue, delirium, seizures, and difficulty breathing [4].

Currently, artemisinin-based combination therapies (ACTs) are the mainstay in malaria treatment [5, 6]. Treatment with these drugs, as well as malaria prevention using malaria vaccine (RTS, S/AS01), is believed to pave way for malaria eradication [7]. Although there has been considerable advancement in the efforts to eradicate malaria over the last 15 years, the goal of global eradication remains unattainable due to recent reports of drug resistance coupled with the challenge of poor drug absorption after oral administration [8]. Despite enormous efforts being put in place in drug discovery for antimalarial drugs and newly discovered mechanisms of action of antimalarial agents, *Plasmodium falciparum*, the deadliest strain of the malaria parasite, has developed resistance to several antimalarial medications [9–21]. The ACT merges rapidly acting artemisinin-derived compounds with a drug from a different class, delivering a powerful dual attack against the malaria parasite [22]. Unfortunately, literature has established that artemisinin-based drugs have poor aqueous solubility as well as low oral bioavailability, and these have put the drugs in a danger list of therapeutic failure, if urgent action is not taken [23].

Artemether, a methyl ether derivative of artemisinin, is a prodrug that is extracted from the Chinese antimalarial plant *Artemisia annua*. It metabolizes to dihydroartemisinin in the bloodstream before attacking the malaria parasite. The drug exerts its anti-malarial effect via iron-catalyzed production of a carbon-centered free radical and subsequent alkylation of malaria-specific proteins [24]. Put another way, its mode of action is the production of alkylated heme and proteins by the heme-mediated breakdown of carbon-centered free radicals [25]. Artemether is transformed into free radicals and other electrophilic intermediates in the presence of intraparasitic iron, which subsequently alkylates particular malaria target proteins [26]. It has been demonstrated that artemisinin can be bioactivated by both heme and free intracellular reduced iron species. This is necessary

for the medication to bind covalently to macromolecules throughout the entire parasite. Thus, artemether covalently alters several targets [27]. Therefore, peroxide in the chemical structure of artemether is essential to its function. First synthesized in the early 1970s, artemether has remained very relevant in the treatment of malaria till date [28]. However, artemether, though very efficacious against malaria parasite has a major drawback of having a short half-life. It is also hydrophobic, grouped under class IV of the biopharmaceutical classification system (BCS). Drugs in this class exhibit an oral bioavailability of about less than 40% due to poor water solubility [29], and are generally not suitable for oral administration unless they are formulated using some special drug delivery technologies [30]. These weaknesses of artemether in addition to the use of substandard artemisinin-based formulations are threats to the progress made in the fight against malaria, by helping early development of drug resistance and recrudescence.

The afore-mentioned setbacks have warranted the modification of the physicochemical properties of the drug using nanotechnology. We intend to use nanotechnology to design an artemether formulation with improved water solubility and oral bioavailability for malaria treatment. In our research, we developed and evaluated artemether-loaded chitosan-modified solid lipid nanoparticles (SLNs) based on solidified reverse micellar solution (SRMS). SRMS are lipid-based biodegradable matrix drug delivery systems widely investigated as potential drug delivery systems for drugs experiencing penetration and absorption challenges [31]. Interestingly, a good number of research has revealed that co-formulation of poorly water-soluble drugs with lipid-based matrices such as SRMS has potential of improving oral bioavailability [30–33]. When lipophilic drugs are incorporated into lipid-based drug delivery systems such as SRMS, their aqueous solubility, absorption and systemic distribution are enhanced. The activities of some enzymes (lipase) and bile salt solubilization in the small intestine on lipids are extended to the lipophilic drugs in their company [34, 35]. SRMS is also used to achieve controlled release of entrapped drugs through a mesophasic transformation of the solid lipid contents after melting and dispersing in water [30, 33].

SRMS-based SLNs offer several advantages including small size and large surface area, controlled drug release, excellent physical stability, prevention of drug degradation, allows for hydrophilic and/or hydrophobic drugs incorporation; avoidance of use of organic solvents for production (hence it is safer); can be used for dermal, per oral, intravenous administration, and most importantly, greater stability and bioavailability of incorporated drug(s) [36, 37]. The main disadvantage of SLNs,

however, is their solid lipid content, which reduces their ability to load drugs since the drugs are ejected from the crystalline structure of the solid lipid [38]. Furthermore, SLNs are susceptible to gastrointestinal fluid and may be destroyed by bile salts due to their lipidic nature [39]. To address these problems, some researchers have employed chitosan as a coating material for SLNs [40–42]. More recently, our group successfully used chitosan as a coating agent for SLNs [43]. This is because chitosan coating can maximize drug transport by preserving the nanostructure of the SLNs and conferring a mucoadhesive effect on the SLNs, thereby increasing the retention of encapsulated drug in the biological membrane.

Chitosan is a natural polymer which contains β -(1,4)-2-acetamido-D-glucose and β -(1,4)-2-amino-D-glucose unit, and is produced from chitin (in shells of crustacea, the cuticles of insects, and cell walls of some fungi) through the removal of an acetate moiety from chitin through hydration in concentrated alkali [44–46]. Chitosan and its derivatives are soluble in dilute acid and its derivatives have different molecular weights and degree of deacetylation, and these properties determine their physical and chemical properties [47]. It is able to form films easily, and hence useful for coating lipids and polymer carriers [48]. Chitosan and its derivatives are very attractive for the formulation of novel drug delivery systems, because of their biodegradability, biocompatibility, versatility of application, enhanced stability and solubility, low toxicity, simple and mild preparation methods [49, 50]. They are therefore used for loading protein drugs, genes, and anticancer drugs; in brain targeting drug delivery, in mucosal drug delivery and for achieving controlled drug delivery [51–53]. Chitosan-based delivery systems have also been useful for various routes of administration including oral, nasal, ocular, vaginal and parenteral routes [40–53].

Meanwhile, there is currently no report on SRMS-based chitosan-coated SLNs containing artemether. Thus, the novelty of this study lies in the use of SRMS-based chitosan-coated SLNs for the first time to enhance oral delivery of artemether for malaria therapy. The chitosan-coated SLN should be capable of protecting artemether against GIT degradation, enhance the amorphosity and hence improve the drug dissolution in biorelevant media and ultimately enhance the antimalarial activity of the drug.

Consequently, the aim of this study was to encapsulate artemether in SRMS-based SLNs and coat the formulation with chitosan in order to improve the water solubility, oral absorptivity and bioavailability of the drug. Uncoated formulations were also formulated for comparison. In vitro characterization was done on the developed formulations to determine the physicochemical

performance; the in vivo antimalarial activity was evaluated in *Plasmodium berghei*-infected mice using a conventional protocol; while histological and hematological effects of the formulations were ascertained in major organs implicated in malaria in comparison to a pure sample of artemether.

Methods

Chemicals

The pure sample of artemether used was a kind gift from May and Baker PLC, Ikeja, Lagos, Nigeria. Soluplus[®] (polyvinylcaprolactam-polyvinyl acetate-polyethylene glycol grafted copolymer) was kindly provided by BASF (Ludwigshafen, Germany). Compritol[®] ATO 888 was kindly provided by Gattefosse (St. Priest, France). Chitosan (200–300 kDa, deacetylated degree 85%) was purchased from Sigma-Aldrich (Gillingham, UK). Other materials include methanol and ethanol (Sigma Aldrich, USA), sorbic acid (Foodchem Int. Co., China), Polysorbate[®] 80 (Tween[®] 80) (Merck KGaA, Darmstadt, Germany), Phospholipon[®] 90G (P90G) (Phospholipid GmbH, Köln, Germany) and Softisan[®] 154 (Cremer Oleo GmbH, Hamburg, Germany). The remaining substances, reagents, and solvents were all purchased commercially and were of analytical grade or above.

Instruments or equipment

The following items of equipment were used in the study: Ultra-Turrax homogenizer (T 25 digital Ultra-Turrax IKA, Staufen, Germany), Nano-ZS zeta sizer equipped with Zeta sizer software v6.34 (Malvern Instruments, United Kingdom), microconcentrator (5000 MWCO Vivascience, Hanover, Germany), freeze-dryer (Amsco/Finn-Aqua Lyovac GTZ, Germany), Fourier transform infrared spectroscope (Perkin-Elmer, MA, USA) equipped with a universal attenuated total reflectance (ATR) sampling attachment (ATR-FTIR), scanning electron microscope (model HITACHI SU3900, JAPAN), diffractometer (D8 Powder Diffractometer, Bruker, USA), UV–Vis Spectrophotometer (Unico 2102 PC UV/Vis Spectrophotometer, New York, USA), centrifuge (TDL-4 B. Bran Scientific and Instrument Co., London, England), pH meter (Hanna Instruments, Romania) Moticom Images Plus 2.0 digital camera (Motic China Group Ltd.) and Statistical Package for Social Sciences, SPSS (Version 17, SPSS Inc., New York, USA).

Quantification of artemether

The analysis of artemether was carried out using an indirect spectrophotometric (Unico 2102 PC UV/Vis Spectrophotometer, New York, USA) method, which was based on reacting a solution of artemether in methanol with concentrated HCl acid and heating at 60 °C for

30 min. The solution was then scanned in the spectrophotometer in the range 200–600 nm and the maximum absorption was observed at 265 nm. Stock solution of the drug in methanol was prepared and diluted in the range of 0.2–1.2 mg/ml followed by dilution with conc. HCl at 1:1 ratio (volume by volume) and heating for 30 min. Absorbances were determined at 265 nm against the blank and then plotted against the corresponding concentrations to give the calibration curve. Thereafter, the method was validated by checking for its precision, accuracy, % recovery, limit of detection and limit of quantitation using standard guidelines. The method exhibited a limit of detection (LOD) of 0.15 µg/mL and a limit of quantitation (LOQ) of 0.69 µg/mL for artemether. The % Drug Recovery, which was 98.5% met the standard accuracy criteria outlined in USP40, NF35 General Chapter 1225 (80–120%). The UV–Vis spectrophotometric system displayed linearity over the concentration range of 10–120 µg/mL ($r^2=0.9984$). Precision, evaluated as %RSD, was consistently less than 2%, indicating a high level of accuracy and reliability in the quantification of artemether. Thus, this method achieved satisfactory percentage recovery, detection and quantitation limits for artemether.

Screening of different solid lipids

In this study, the solubility of artemether in the solid lipids [stearic acid (SA), Softisan[®] 154 (S154) and Compritol[®] 888 ATO (C888)] was determined using modifications of established techniques [54, 55]. Briefly, excess amounts of artemether were added to each melted lipid (after heating at 10 °C above their melting temperatures) until saturation was reached. In addition, using 1:3 (w/w) drug-lipid ratio, artemether was added to each melted lipid (after 15 min heating at 10 °C above their melting temperatures) and stirred for 5 min in a thermostated magnetic stirring plate assembly. Thereafter, the drug-lipid mixture was visually inspected. The clarity of the drug-lipid mixture played a role in the selection of the lipid in addition to the saturation solubility of the drug in the lipid.

Formulation of SRMS lipid matrices

Following the solubility test performed in the preceding section, C888 (m.p. 75 °C) was selected for the preparation of the solidified reverse micellar solution (SRMS) lipid matrices consisting of 30:70 mixtures of Phospholipon[®] 90G (P90G) and Compritol[®] 888 ATO (C888) by the fusion method [39]. P90G and C888 were weighed precisely, melted together at 85 °C on a hot plate, and agitated at 200 rpm with the aid of a magnetic bead. After melting and mixing, the temperature was lowered to room temperature to allow the lipid matrix to solidify.

It was then scraped out of the beakers and kept in tightly sealed glass bottles until needed.

Preparation of SRMS-based artemether-loaded chitosan-coated SLNs

The SLN formulations were prepared by a high-speed homogenization method [56]. In these formulations, the lipid matrix prepared from P90G and C888 were used in addition to Tween[®] 80 (surfactant), sorbic acid (preservative), Soluplus[®] (solubilizer/co-surfactant) and distilled water (vehicle) with or without chitosan by the high-speed melt-emulsification technique. The lipid phase, which included artemether (1.0%w/w), was mixed with the aqueous phase, which contained an emulsifier, to prepare the formulation. A hot plate magnetic stirrer was used to continuously stir a known volume of distilled water at 1,000 rpm while maintaining a temperature of 85 °C. Tween[®] 80, sorbic acid, and Soluplus[®] were added to the mixture to prepare the aqueous phase. The lipid phase was prepared by melting the lipid matrix composed of P90G and C888 at 85 °C and dissolving artemether in it. The aqueous phase was dropwise mixed with the lipid phase at the same temperature of both phases, i.e., 85 °C with constant stirring for 30 min. The primary emulsion obtained was then subjected to high-speed homogenization using the Ultra-Turrax homogenizer (T 25 digital Ultra-Turrax IKA, Staufen, Germany) for 15 min at 10,000 rpm. The final formulation was then immediately cooled at 10 °C using an ice bath to obtain SLNs. For chitosan-coated SLN formulations, a specified amount of chitosan (0.5%) was added to the aqueous phase. Briefly, after being dissolved in 1% acetic acid solution, the chitosan was added to the aqueous phase, which also contains the surfactants (Table 1).

Determination of mean particle sizes, polydispersity indices and zeta potential

Polydispersity indices (PDI), zeta potential, and hydrodynamic mean particle size of the formulations were measured at 25 °C using a Nano-ZS zeta sizer equipped with Zeta sizer software v6.34 (Malvern Instruments, United Kingdom). The instrument utilizes a 4 mW He–Ne red laser at 633 nm. The light scattering was detected at 173° by non-invasive backscatter technology with a measuring range from approximately 0.6 nm to 6 µm. Disposable polystyrene cuvettes (1 ml) were used for measurements. Double distilled water was used to dilute the formulations and measurements were done in triplicates.

Determination of encapsulation efficiency (EE) and loading capacity (LC)

A microconcentrator (5000 MWCO Vivascience, Hanover, Germany) was filled with about 5 ml of each of the

Table 1 Formulation composition of artemether-loaded SRMS-based chitosan-coated SLNs

Batch code	Lipid matrix (%w/w)	Artemether (%w/w)	Tween® 80 (%w/w)	Soluplus® (%w/w)	Sorbic acid (%w/w)	Chitosan (%w/w)	Distilled water q.s. to 100%w/w
X ₁	10.0	1.0	1.0	4.0	0.1	0.0	100.0
Y ₁	10.0	1.0	1.0	4.0	0.1	0.5	100.0
X ₀	10.0	0.0	1.0	4.0	0.1	0.0	100.0
Y ₀	10.0	0.0	1.0	4.0	0.1	0.5	100.0

X₀ free neutral SRMS-based SLNs, Y₀ free chitosan-coated SRMS-based SLNs, X₁ artemether-loaded unmodified SRMS-based SLNs, and Y₁ artemether-loaded chitosan-coated SRMS-based SLNs

uncoated and chitosan-coated SLNs. After centrifuging the microconcentrator (TDL-4 B. Bran Scientific and Instrument Co., London, England) for two hours at 4000 rpm, the supernatant was collected and diluted with methanol followed by addition of concentrated HCl acid and heating at 60 °C for 30 min. The drug concentration was sufficiently assessed using spectrophotometry at a preset wavelength (Unico 2102 PC UV/Vis Spectrophotometer, New York, USA). Equation 1 was used to compute the quantity of artemether encapsulated in the SLNs using the typical Beer-Lambert's plot for artemether to determine the EE % [37].

$$EE (\%) = \frac{\text{Actual drug content}}{\text{Theoretical drug content}} \times 100 \quad (1)$$

Using Eq. 2, the ratio of the lipids' overall weight to the active pharmaceutical ingredient (API) that is entrapped is expressed by LC [57].

$$LC = \frac{W_a}{W_l} \times 100 \quad (2)$$

where, W_l is the weight of lipid added in the formulation and W_a is the amount of API entrapped by the lipid.

Lyophilization of artemether-loaded chitosan-coated SRMS-based SLN dispersions

For the purpose of performing solid-state and other characterizations, the formulated samples were divided into two and one part was lyophilized. In short, the samples underwent a 12-h lyophilization process in a freeze-dryer (Amsco/Finn-Aqua Lyovac GTZ, Germany) set at -40 °C and 2.7 Pa of pressure; the lyophilized powders of the uncoated and chitosan-coated SLNs were then stored in a dry, cool area.

Fourier transform infrared (FT-IR) spectroscopy

Utilizing attenuated total reflectance, the compatibility between the pure drug and excipients was investigated using a PerkinElmer Spectrum equipped with a universal attenuated total reflectance (ATR) sampling attachment, Fourier transform infrared spectroscopy (ATR-FTIR)

(Perkin-Elmer, MA, USA). In short, the spectra manager set up the proper parameters after the equipment had been equilibrated for thirty minutes. The ATR crystal (ZnSe) was coated with a 2 mg quantity of artemether and an optimized lyophilized formulation (artemether-loaded chitosan-modified SLNs). The screw unit of the ATR was then tightened clockwise until it made contact with the sample. The upper cabinet was closed in order to measure the sample spectra via the computer monitor. FT-IR spectra were obtained after an aggregation of 16 scans, with the range of 4000 to 400 cm⁻¹ at room temperature.

Scanning electron microscopy analysis of the artemether-loaded chitosan-coated SLNs

The morphological features of the artemether-loaded uncoated and chitosan-coated SLNs were assessed by scanning electron microscopy (SEM) analysis at PSU (Prince of Songkla University), Thailand. Prior to assessment, the samples were sputter-coated with gold in a sputter (SPI supplies, USA) and mounted on aluminum stubs using adhesive carbon tape. Images were then taken using a scanning electron microscope (model HITACHI SU3900, JAPAN) operating at 15 kV.

Powder X-ray diffractometry

X-ray diffraction patterns of artemether and optimized formulation (artemether-loaded chitosan-modified SLNs) were recorded using a diffractometer (D8 Powder Diffractometer, Bruker, USA) to investigate their crystal properties. Measurements were performed at room temperature while the samples were subjected to Cu K α radiation (40 kV, 35 mA) [58]. For each sample, scanning was done at 2 θ diffraction angle in the range of 5–90°.

In vitro drug release study

The in vitro release of artemether from artemether-loaded SLNs and chitosan-coated artemether-loaded SLNs was investigated via a dialysis method [59]. A volume of roughly 5 ml for every formulation was put into a polycarbonate dialysis membrane bag that had been pre-treated (molecular weight cut-off of about

6000–8000 Da) and sealed hermetically at both ends. The dialysis bag was then placed inside a beaker containing 200 ml of the release medium (phosphate buffered saline, or PBS) with a pH of 6.8, 0.5% (v/v) Tween 80). Next, the dialysis bag was placed inside a thermoregulated water bath and agitated at 100 rpm at 37 °C. To keep a sink condition, a succession of 1 mL quantities of the release media was removed at different intervals and then replaced with an equivalent volume of fresh medium. To ascertain the quantities of artemether, the extracted samples were derivatized with methanolic HCl at 60 °C for 30 min, diluted, and examined at a preset wavelength using the UV–vis spectrophotometer. After that, the amount of artemether released cumulatively at each determination was calculated. The release study was carried out in duplicates throughout.

In vivo antimalarial studies

Ethical approval

The animal experimental protocols were in accordance with the guidelines for conducting animal experiments stipulated and approved by our Institution's Animal Ethics Committee (Faculty of Pharmaceutical Sciences Research Ethics, approval n. FPSRE/UNN/20/00064) and in compliance with the Federation of European Laboratory Animal Science Association and the European Union Directive 2010/63/EU for animal experiments.

Animals and parasite

In this study, locally raised albino (BALB/c) mice of both sexes (male and female) that appear to be in good health, 8–10 weeks old, with weights ranging between 16 and 21 g were used. The animals were acquired from the University of Nigeria, Nsukka's Faculty of Veterinary Medicine, and were first kept in a room in the animal house. Metallic and plastic cages were used to keep the animals, and they were cleaned and had new bedding on a regular basis. The experimental mice were maintained at ambient temperature and humidity levels, with a 12-h light/dark cycle as well as on a normal diet of commercial livestock feed with unlimited access to water.

The rodent malaria parasite used was NK-65 strain of *Plasmodium berghei*. This strain is highly infective in mice with life cycle that is essentially similar to human malaria parasite. It causes lethal infections in mice with high mortality rates and is sensitive to all currently used antimalarial drugs, providing a good model to estimate the efficacy and survival [60]. The parasite was obtained from the Institute of Medical Research and Training, University College Hospital (UCH), Ibadan, and it served

as a model for *Plasmodium falciparum*, which is responsible for human malaria [61].

Preparation of inoculum

By repeated passaging, blood drawn from a donor mouse was diluted with normal saline to provide a standard inoculum of 1×10^7 parasitized erythrocytes [62, 63]. Briefly, a stock parasitized erythrocytes was obtained from infected mice, with a minimum peripheral parasitemia of 20% through the retro-bulbar plexus of the median canthus of its eye. The blood was collected into an EDTA-coated tube. The percentage parasitemia in each case was determined by counting the number of parasitized red blood cells against the total number of red blood cells. The cell concentration of the stock was determined and diluted with normal saline such that 0.2 ml of the final inoculums contained 1×10^7 parasitized red blood cells which are the standard inoculum for the infection of a single mouse.

Experimental protocol

Eighteen mice were divided into 3 groups of six mice each as shown in Table 2. The mice groups (A-C) were infected with chloroquine-sensitive strain of *Plasmodium berghei* (CPb) as described in the preceding section. Five days after the inoculation of the mice with CPb, percentage parasitemia was determined and, after the establishment of malaria, treatment was started on the same day (day 1) on the malariogenic mice and was repeated till day 3. Details of the experimental treatments are shown in Table 2. Parasitemia was assessed from tail blood smears (Giemsa-stained) post treatment. Blood samples were taken from the mice's tails, and after fixing the blood with methanol and staining it with 10% Giemsa, thin blood films were produced. Slides for the parasite from each groups were prepared, stained with blood smear and placed under a binocular microscope with an immersion oil droplet applied to it [64]. Red blood cells (RBCs) with and without parasites were analyzed microscopically ($\times 1000$ magnification) in each slide field. The total number of RBCs was calculated by counting the number of parasitized RBCs in each field. Equations 3 and 4 were used to compute the mean parasitemia (%) and the percentage reduction in parasitemia [9].

Table 2 Treatments administered to the mice perorally

Group	Sample code	Treatment	Dosing
A	Art-loaded CS-SLNs	Optimized formulation	10 mg/kg \times 3 days
B	Art pure sample	Positive control	10 mg/kg \times 3 days
C	Unloaded CS-SLNs	Placebo (negative control)	2 ml/kg \times 3 days

Art is artemether; CS-SLNs is chitosan-coated solid lipid nanoparticles

$$\text{Mean parasitemia}(\%) = \frac{\text{Number of infected red blood cells(RBCs)}}{\text{Total number of RBC count}} \times 100 \quad (3)$$

$$\text{Percentage reduction in parasitemia}(\%) = \frac{\text{Parasitemia of negative control}(\%) - \text{Parasitemia of treated group}(\%)}{\text{Parasitemia of negative control}(\%)} \times 100 \quad (4)$$

Determination of hematological parameters

Samples of blood were taken from the tails of every mouse (before inoculation with the malaria parasite to get the baseline, after the establishment of parasitemia, and post-treatment for the treatment groups) and evaluated with respect to packed cell volume (PCV) and hemoglobin (Hb) using an auto analyzer, consistent with an established procedure [65].

Weight determination

The various weights of the mice were determined before inoculation, after establishment of parasitemia, and after treatment to assess the effect of the parasitemia and the treatments on the weights of the animals. The mean body weights for the groups were calculated.

Assessment of *Plasmodium berghei*-induced lethality in mice

In order to determine the survival rate of mice treated with the formulations, the number of infected mice that died from *Plasmodium berghei* infection was used to determine the lethality of the illness.

Histopathological studies

At the end of the experiment, all mice were euthanatized by cervical dislocation and a mouse from each group was used for histopathological studies. Samples from the kidneys and liver of mice treated with optimized sample, control and placebo were collected and fixed with 10% neutral-buffered formalin, dehydrated in graded concentrations of ethanol, cleared in xylene and embedded in paraffin wax. Sections with a thickness of around 5 μm were cut, put on a glass slide, and then stained with hematoxylin and eosin (H & E). A Leica binocular light microscope was coupled with a Moticam Images Plus 2.0 digital camera (Motic China Group Ltd.) to take the photomicrographs of the sections [55].

Cytotoxicity test

The cytotoxicity test was conducted on the optimized artemether-loaded chitosan-coated SLNs by measuring the viability of the cells using the 3-(4,5-dimethyl-2-thiazolyl)-2,5-diphenyl-2H-tetrazolium bromide (MTT) assay, with minor modifications [66]. Briefly, 200 μL of growth media was added to 96-well plates, where 1×10^3 cells were planted per well. The plates were then placed in a humidified incubator at 37 $^{\circ}\text{C}$ with 5% CO_2 . After the cells were cultured for 48 h, the culture medium was removed, and 100 μL of the test solutions (optimized artemether-loaded chitosan-coated SLNs and plain chitosan-coated SLNs acting as placebo) and negative control (100 μL of culture medium) were added to the wells. The culture medium was mixed with the test solutions, and the mixture was then further cultured for 24 h. Subsequently, each well was filled with 15 μL of 2.5 mg/mL MTT solution, and the cells were stained for 4 h at 37 $^{\circ}\text{C}$. After the medium was removed, 100 μL of dimethyl sulfoxide (DMSO) was added to each well, and the absorbance was measured at 503 nm. Finally, the relative cell viability (%) was computed using Eq. 5.

$$\text{Cell viability \%} = \frac{\text{absorbance of sample cells}}{\text{absorbance of control cells}} \times 100\% \quad (5)$$

Stability studies

The pH of the formulations was determined in a time-dependent manner after 1 day, 1 week, 1 month and 3 months of storage at ambient temperature (28 ± 3.0 $^{\circ}\text{C}$). Briefly, the pH of the formulations was measured potentiometrically (Hanna Instruments, Romania) at room temperature. The electrode of the pH meter was inserted into each formulation thrice and mean pH value recorded after calibrating with standard buffer. The pH was re-evaluated after 1, 7, 30 and 90 days. To determine whether the particle qualities of the formulations had changed, a storage stability study was also conducted on them. For a duration of 6 months, the samples were kept at room temperature

(28 ± 3.0 °C) in an airtight container. Thereafter, the samples were reassessed using the zeta potential, mean particle size, and polydispersity index as mentioned in the previous sections.

Statistical analysis

Results were shown as mean \pm SEM and data sets were analyzed using SPSS (Version 17, SPSS Inc., New York, USA). The data sets from animal experiments were analyzed on GraphPad prism 10.3, using ordinary one-way or two-way analysis of variance (ANOVA) followed by Tukey's multiple comparisons test. Values were expressed as mean \pm SEM (standard error of means) of $n=6$. A P value less than 0.05, 0.01, 0.001 and 0.0001 was considered statistically significant and was flagged with one star (*), two stars (**), three stars (***), and four stars (****), respectively.

Results

Solubility of artemether in the solid lipids

The results of the solubility test carried out on the drug in the solid lipids are presented in Table 3. Results indicate that C888 showed the best solubility of artemether followed closely by S154 and lastly by SA. The saturation solubility of artemether in C888, S154 and SA were 21.6 ± 0.32 ,

Table 3 Solubility of artemether in the solid lipids

Lipid	Solubility	
	Visual inspection	Saturation solubility (mg/g)
Compritol® ATO 888	++++	21.6 ± 0.32
Softisan® 154	+++	15.9 ± 0.81
Stearic acid	++	10.2 ± 0.54

+ Sparingly soluble, ++ Slightly soluble, +++ Soluble, ++++ Freely soluble, – not soluble

Table 4 Physicochemical properties of artemether-loaded chitosan-coated SRMS-based SLNs showing particle properties as well as loading capacity and EE

Sample	Z-Av (nm)		PDI		ZP (mV)		EE (%)	LC (%)
	1 week	6 months	1 week	6 months	1 week	6 months		
X ₀	286.20 ± 3.09	284.05 ± 2.16	0.275 ± 0.08	0.205 ± 0.06	-15.55 ± 0.99	-16.08 ± 1.03	–	–
Y ₀	326.65 ± 4.18	327.42 ± 5.07	0.286 ± 0.03	0.198 ± 0.02	$+28.65 \pm 1.34$	$+30.12 \pm 1.89$	–	–
X ₁	246.75 ± 2.97	248.34 ± 3.65	0.200 ± 0.07	0.298 ± 0.05	-30.70 ± 1.06	-31.83 ± 2.16	81.96	10.67
Y ₁	292.90 ± 5.01	293.78 ± 4.09	0.191 ± 0.09	0.219 ± 0.04	$+32.50 \pm 1.58$	$+34.19 \pm 1.82$	82.03	11.23

X₀ unloaded unmodified SRMS-based SLNs, Y₀ unloaded chitosan-coated SRMS-based SLNs, X₁ artemether-loaded uncoated SRMS-based SLNs, and Y₁ artemether-loaded chitosan-coated SRMS-based SLNs. Particle properties were determined within 1 week of formulations preparation and after 6 months of storage at ambient temperature condition ($n=3$)

15.9 ± 0.81 and 10.2 ± 0.54 mg/g, respectively. Therefore, C888 was selected for further formulation studies.

Particle properties of artemether-loaded chitosan-coated SLNs

Table 4 presents the particles properties of the formulations whereas the particle size distribution profile and zeta potential profile of the optimized formulation are presented in Fig. 1a, b, respectively. Results show that the hydrodynamic diameters of plain uncoated and chitosan-coated SLNs were 286.20 ± 3.09 and 326.65 ± 4.18 nm, respectively, with corresponding PDIs of 0.275 ± 0.08 and 0.286 ± 0.03 , respectively, while those of artemether-loaded uncoated and artemether-loaded chitosan-coated SLNs were 246.75 ± 2.97 and 292.90 ± 5.01 nm, respectively, with corresponding PDIs of 0.200 ± 0.07 and 0.191 ± 0.09 , respectively. Besides, Table 4 showed that the superficial charges (zeta potentials) obtained for plain SLNs and artemether-loaded SLNs were -15.55 ± 0.99 and -30.70 ± 1.06 mV, respectively, whereas those of their chitosan-coated counterparts were $+28.65 \pm 1.34$ and $+32.50 \pm 1.58$ mV, respectively. This indicates that the developed formulations had both negative and positively charged particles.

Encapsulation efficiency and loading capacity

Table 4 presents the encapsulation efficiency and loading capacity of artemether-loaded uncoated and chitosan-coated SRMS-based SLNs. According to the table, artemether-loaded uncoated SLNs and artemether-loaded chitosan-coated SLNs gave EE% of 81.96 and 82.03%, respectively, with corresponding loading capacity of 10.67 and 11.23%, respectively.

Powder x-ray diffractometry of artemether-loaded chitosan-coated SLNs

Figure 2a, b depicts the x-ray diffractograms of pure artemether sample and artemether-loaded chitosan-coated SLNs in superposition. Strong reflections at (2θ)

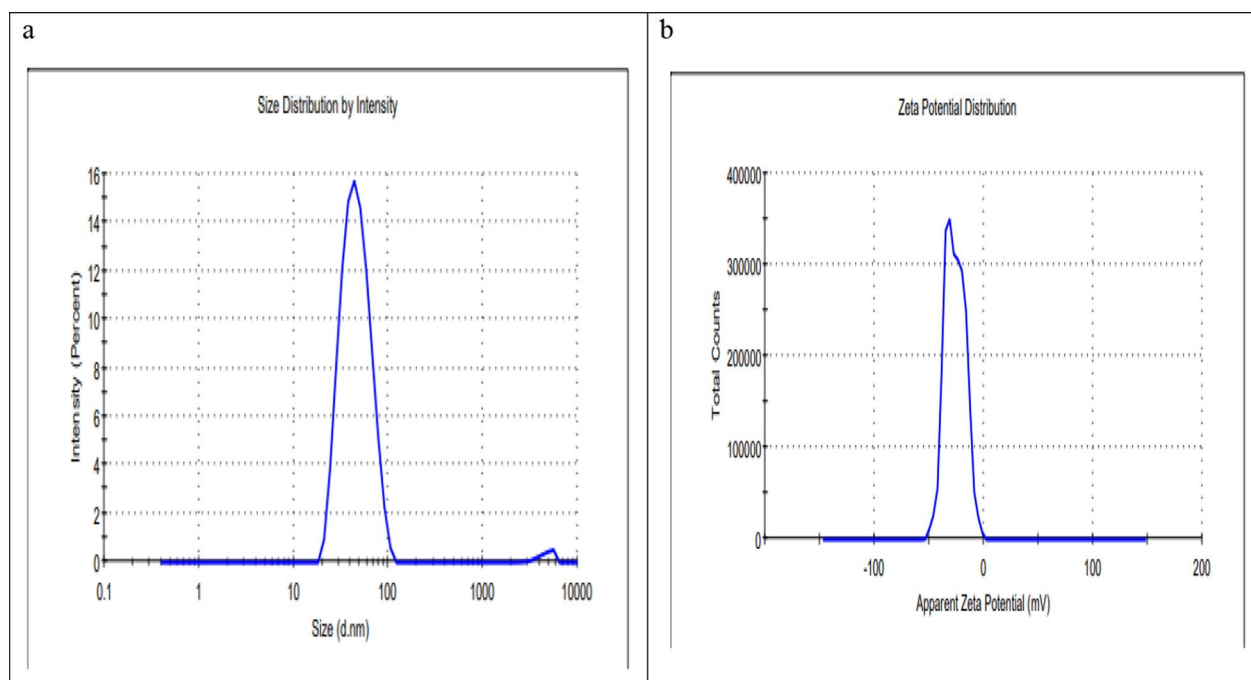


Fig. 1 Particle size distribution profile (a) and zeta potential distribution curve (b) of the artemether-loaded chitosan-coated solidified reverse micellar solution-based solid lipid nanoparticles (optimized formulation)

9.5°, 11.2°, 12.0°, 14.3°, 17.4°, 19.8°, 21.1°, 22.7°, 23.2°, 24.9° and 26.4°, and other reflections of medium and low intensities were seen in the diffractogram of artemether (Fig. 2a). For the artemether-loaded chitosan-coated SLN formulation, strong diffraction peaks were observed at five major peaks, viz (2 θ) 6.7°, 9.5°, 12.3°, 40.8° and 46.1°, alongside other reflections of medium and low intensities (Fig. 2b).

Structure integrity of the drug in the artemether-loaded chitosan-coated SLNs formulation

Figure 3a, b shows the FT-IR spectra of artemether and artemether-loaded chitosan-coated SLNs in superposition. The principal characteristic absorption bands of artemether were revealed by the FT-IR spectrum (Fig. 3a), which included the following: O–H stretching at 3456 cm⁻¹, O=C–H stretching (double bands, weak) at 2940 and 2859 cm⁻¹, C=O functional group at 1750 cm⁻¹, CH₃ bond bending at 1459 and 1425 cm⁻¹, C–O vibration at 1340 cm⁻¹, C–H bending at 1150 and 1097 cm⁻¹, O–O–C stretching at 905 cm⁻¹, and O–O stretching at 751 cm⁻¹. The FT-IR spectrum of the chitosan-coated SLNs loaded with artemether (Fig. 3b) revealed the main characteristic absorption bands of artemether, which included the following: O–H stretching at 3470 cm⁻¹, O=C–H stretching (weak double bands) at 2950 and 2829 cm⁻¹, C=O functional group at 1725 cm⁻¹, CH₃ bond bending at 1458 cm⁻¹, C–O

vibration at 1350 and 1298 cm⁻¹, C–H bending at 1147 and 1080 cm⁻¹, O–O–C stretching at 905 and 826 cm⁻¹, and O–O stretching at 754 and 689 cm⁻¹.

Scanning electron microscopy

The SEM micrographs of uncoated and chitosan-coated SRMS-based SLNs are presented in Fig. 4a, b. Evidently, the uncoated SLNs produced a significant degree of asperity in the form of predominantly irregular, multi-particulate particles (Fig. 4a), whereas chitosan-coated formulations showed well-identified spherical polymer-coated structures (Fig. 4b).

In vitro drug release

Figure 5 presents the in vitro release profiles of unformulated artemether (artemether suspension) and different SLN formulations (artemether-loaded uncoated SLNs and artemether-loaded chitosan-coated SLNs). It could be seen from the figure that artemether showed a significantly higher burst release (33%) after 30 min compared to artemether-loaded SLNs (15%) and artemether-loaded chitosan-coated SLNs (9%). In fact, the percentage of artemether released from artemether suspension reached 100% in 4 h. Following the 12-h release study, the release percentage of artemether was 65.05% for artemether-loaded SLNs and 61.27% for artemether-loaded chitosan-coated SLNs.

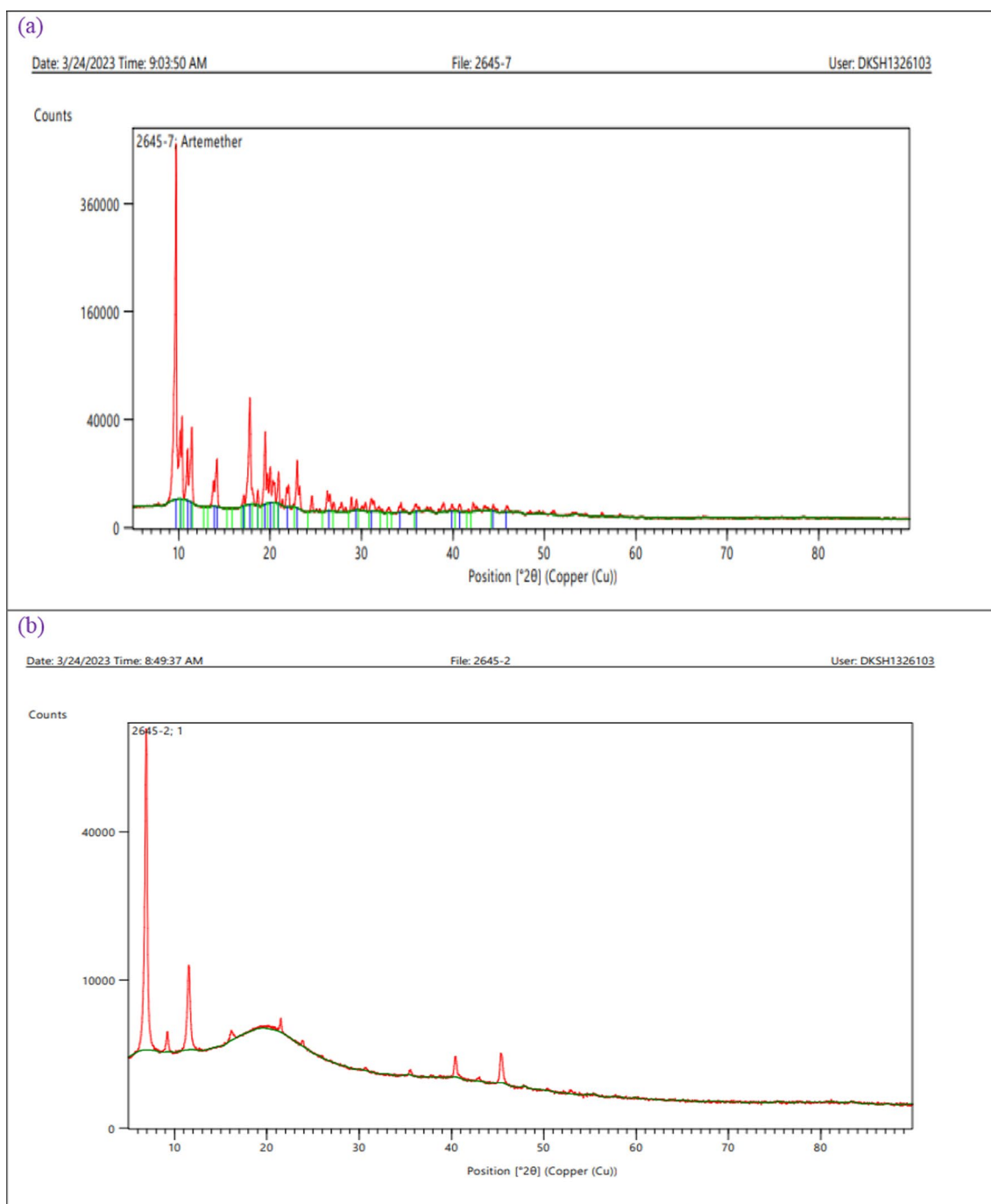


Fig. 2 PXRD diffractogram of **a** pure artemether sample and **b** artemether-loaded chitosan-coated SRMS-based lipid nanoparticles in superposition

In vivo antimalarial activity

The results of the in vivo antimalarial study are presented in Figs. 6 and 7 as mean parasitemia levels in the experimentally *Plasmodium berghei*-infected groups of mice with or without peroral treatment and percentage reduction in parasitemia of mice infected with the parasite after 3 days of peroral treatment, respectively. As

could be seen from the results, artemether-loaded chitosan-coated SLNs showed significantly ($p < 0.05$) greater reduction in mean parasitemia than artemether alone (positive control) and unloaded formulation (placebo or negative control).

The mean parasitemia count of the group treated with the optimized formulation (artemether-loaded

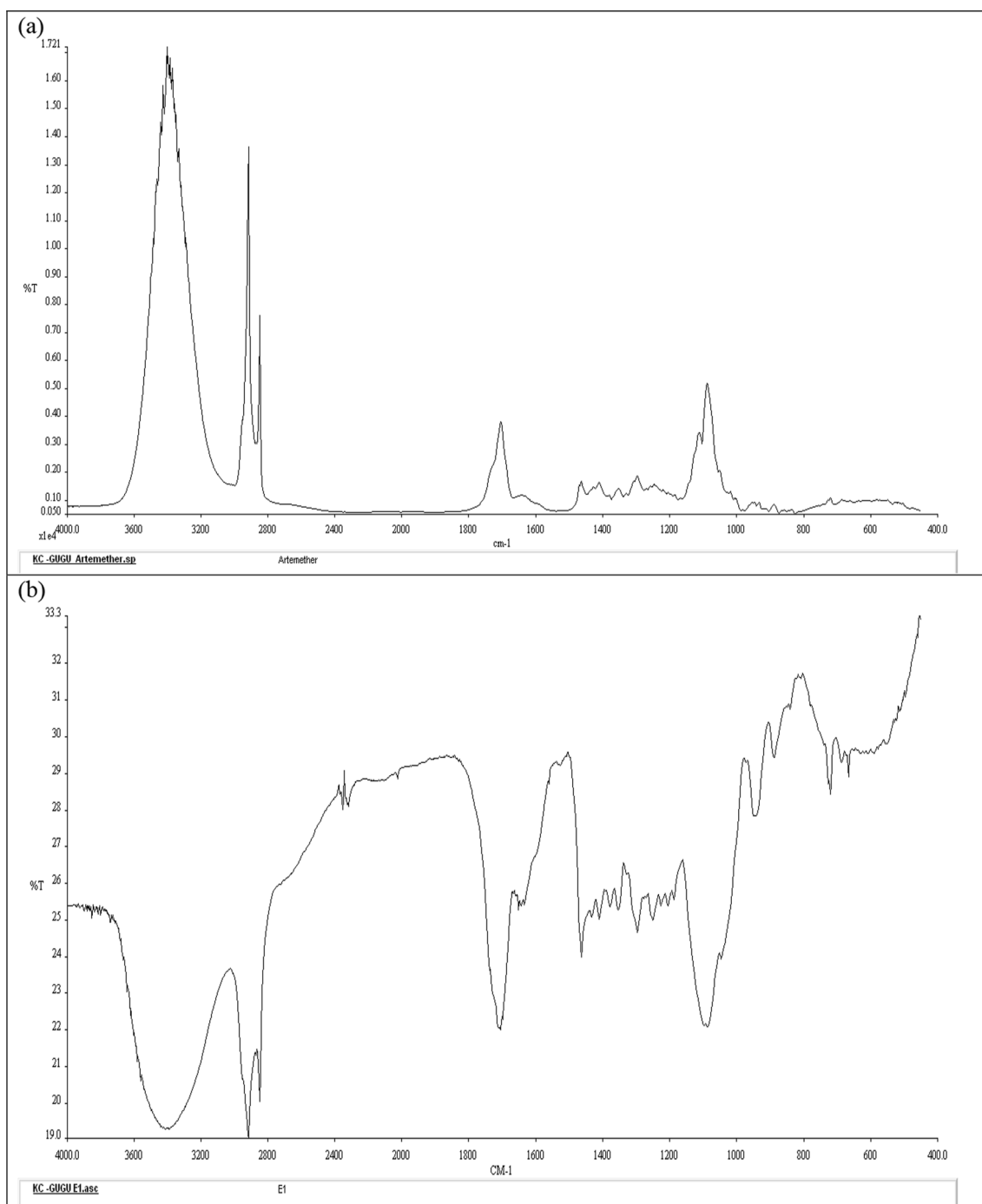


Fig. 3 FT-IR spectra of **a** artemether and **b** artemether-loaded chitosan-coated solid lipid nanoparticles in superposition

chitosan-coated SRMS-based SLNs) decreased from 27 post-inoculation to 19 post-treatment, whereas the group treated with the reference sample (artemether serving as positive control) decreased from 49 post-inoculation to 41 post-treatment (Fig. 6). The placebo group, on the other hand—the group that received

the unloaded formulation, which acted as the negative control—saw an increase in mean parasitemia count from 25 post-inoculation to 41 following treatment. In addition, Fig. 7 demonstrated that the percent parasitemia decrease at study completion (i.e., post-treatment) for the reference sample was 16.41%,

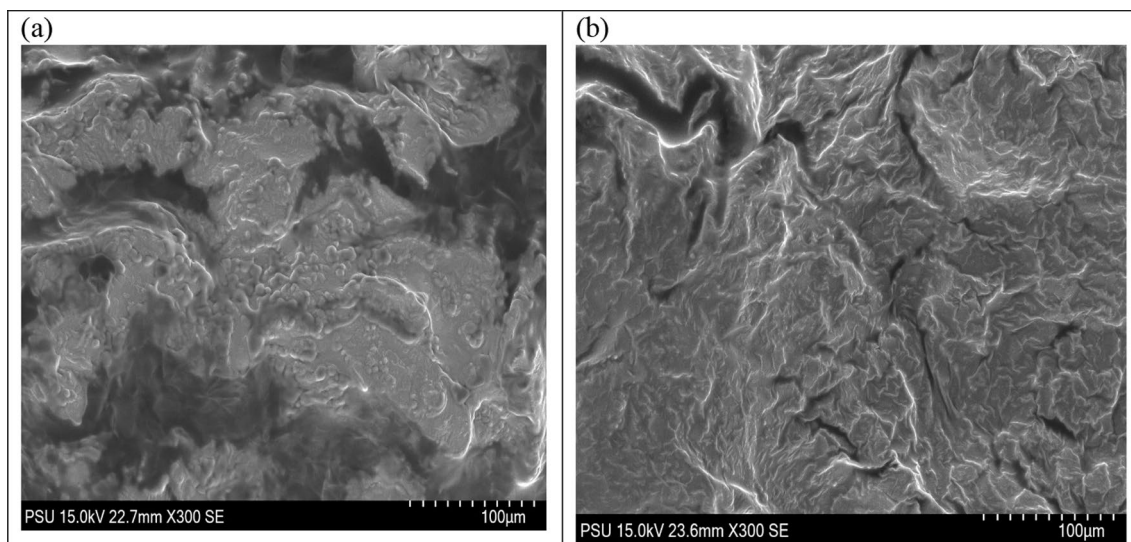


Fig. 4 SEM micrographs of **a** uncoated SRMS-based solid lipid nanoparticles and **b** artemether-loaded chitosan-coated SRMS-based solid lipid nanoparticles

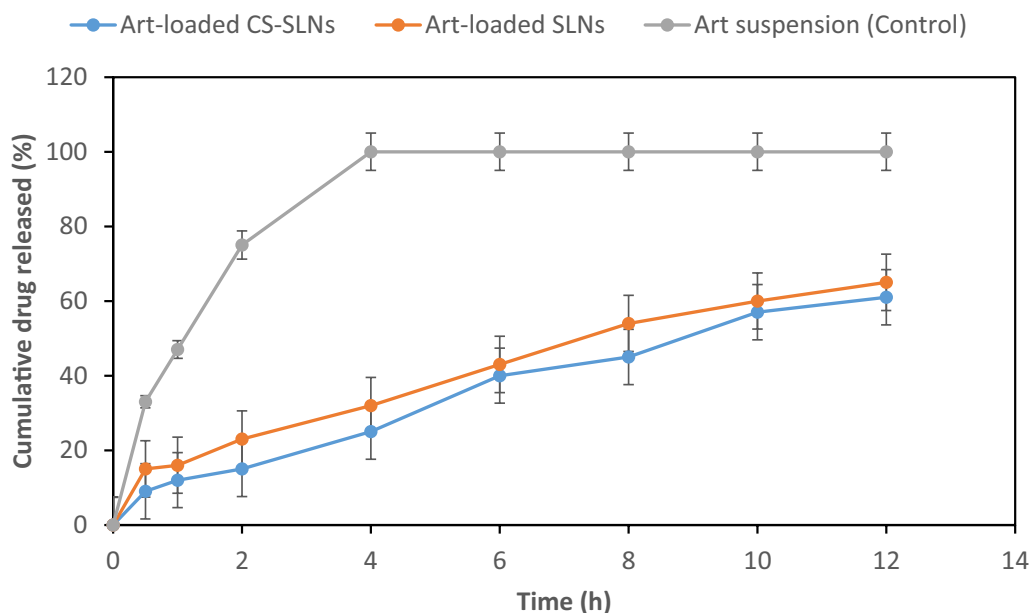


Fig. 5 Release profiles of artemether as pure drug and artemether-loaded uncoated and chitosan-coated SRMS-based SLNs in phosphate buffered saline (pH 6.8) at 37 °C. Data expressed as mean ± SEM, n=3. Key: Art suspension (control) is a dispersion of pure artemether sample, Art-loaded SLNs is artemether-loaded uncoated SRMS-based SLNs, while Art-loaded CS-SLNs is artemether-loaded chitosan-coated SRMS-based SLNs

while artemether-loaded chitosan-coated SLNs recorded a percent reduction of 29.7% post-treatment. This suggests that the formulation has a considerable ($p < 0.0001$) improvement in antimalarial activity. Further information can be found in the supplementary file 1.

Hematological parameters

The hematological parameters [packed cell volume (PCV) and hemoglobin (Hb)] obtained in infected mice treated with the samples are presented in Figs. 8 and 9. Obviously, there was a significant decrease in Hb and PCV in the infected mice group that received the unloaded formulation (negative control), but treatment with artemether-loaded chitosan-modified SLNs (optimized

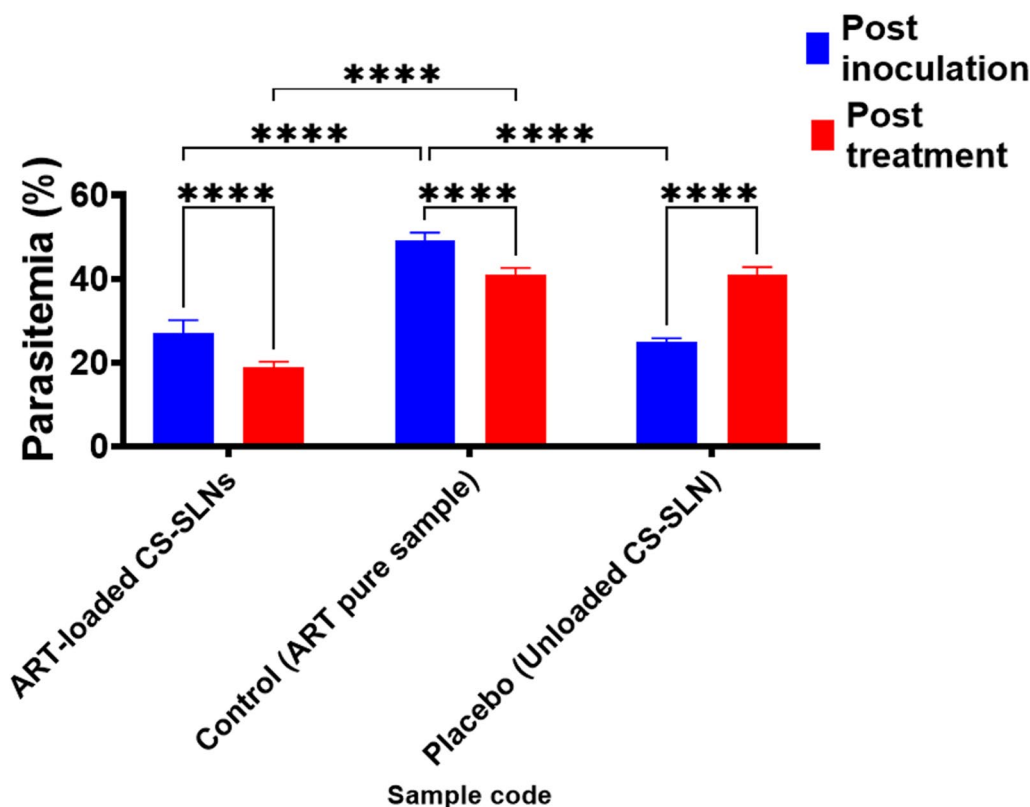


Fig. 6 Mean percentage parasitemia of mice treated with the formulations. Data were expressed as mean ± SEM (standard error of mean) n=6, differences were considered significant for ****p < 0.0001. Key: Post treatment means with peroral treatment, Post inoculation means without peroral treatment, ART pure sample (control) is pure artemether sample, Unloaded CS-SLN is unloaded chitosan-coated SRMS-based SLNs, and ART-loaded CS-SLNs is artemether-loaded chitosan-coated SRMS-based SLNs

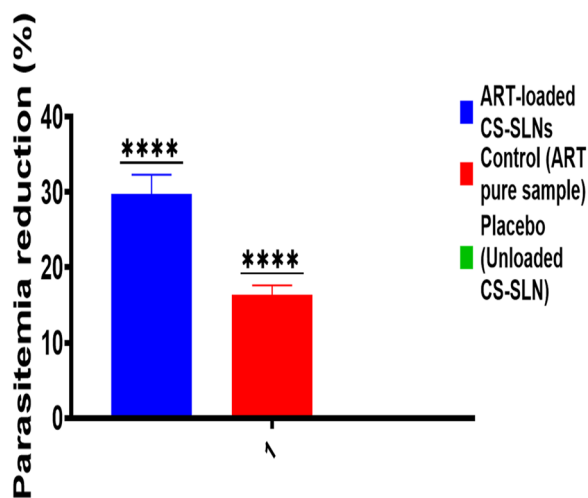


Fig. 7 Reduction in parasitemia of mice treated with the formulations. Data were expressed as mean ± SEM (standard error of mean) n=6, differences were considered significant for ****p < 0.0001. Key: ART pure sample (control) is pure artemether sample, Unloaded CS-SLN is unloaded chitosan-coated SRMS-based SLNs, and ART-loaded CS-SLNs is artemether-loaded chitosan-coated SRMS-based SLNs

formulation) significantly increased the Hb (from 7.4 g/dL to 10.9 g/dL) and PCV (from 29.1 to 38.6%, while treatment with pure artemether sample increased Hb and PCV from 8.1 to 9.8 g/dL and 28.2–34.5%, respectively. Further information can be found in the supplementary file 2.

Weight variation

The weight variation results of the mice infected with *Plasmodium berghei* before and after treatment with the samples are depicted in Fig. 10. The figure could be used to interpret that the weight of the animals varied slightly.

Lethality of infected mice after treatment with artemether-loaded chitosan-coated SRMS-based SLNs
Table 5 presents the lethality results of mice infected with *Plasmodium berghei* after treatment with the samples. In our investigation, there was no record of death in the group that received the optimized formulation (artemether-loaded chitosan-coated SRMS-based SLN) as there was complete recovery of mice at the end of

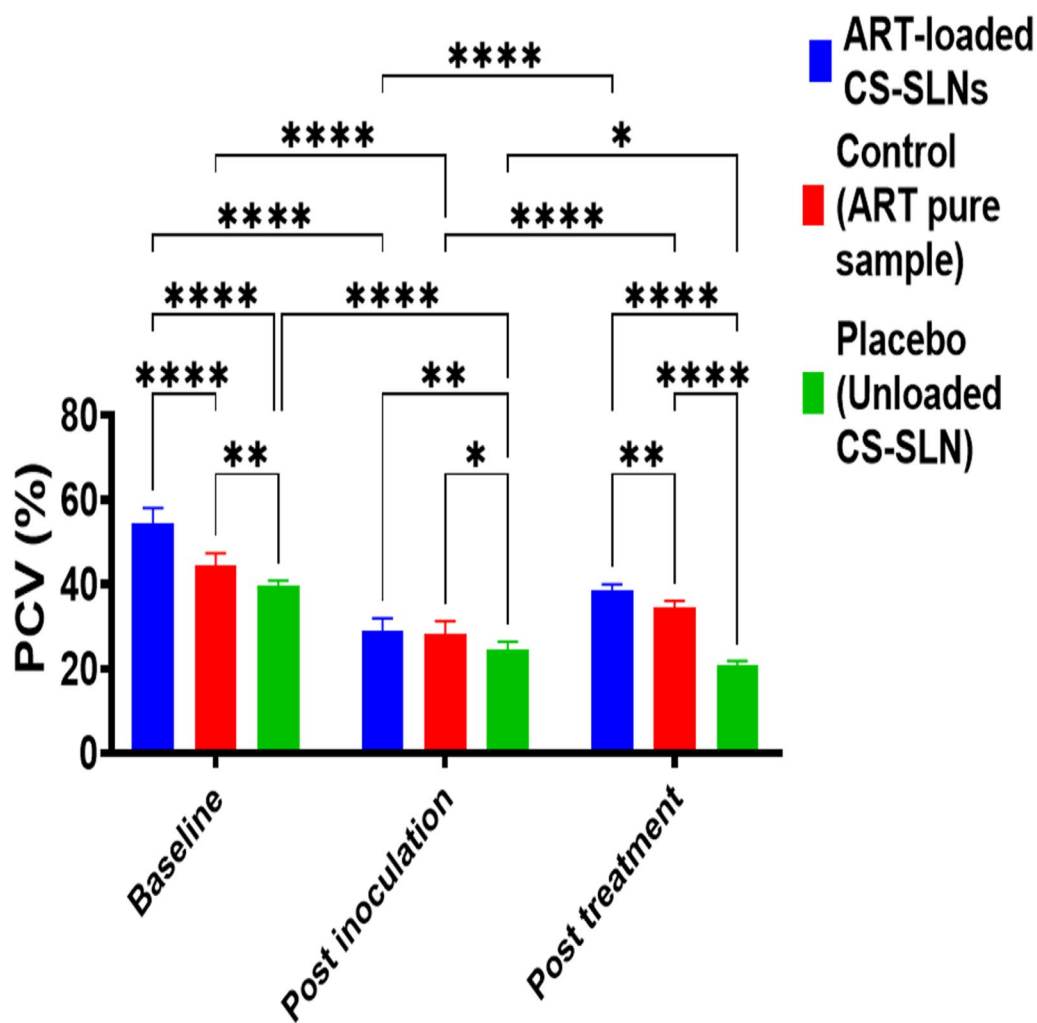


Fig. 8 PCV of mice treated with the formulations. Data were expressed as mean \pm SEM (standard error of mean) $n=6$, differences were considered significant for $*p < 0.05$, $**p < 0.01$ and $****p < 0.0001$. Key: Post treatment means with peroral treatment, Post inoculation means without peroral treatment, ART pure sample (control) is pure artemether sample, Unloaded CS-SLN is unloaded chitosan-coated SRMS-based SLNs, and ART-loaded CS-SLNs is artemether-loaded chitosan-coated SRMS-based SLNs

the experiment. However, 16.67% (1/6) mortality was recorded in the reference group (artemether) while 66.67% (4/6) mortality was obtained in the placebo group (unloaded formulation).

Histopathological studies

The results of the histopathological analysis performed on the liver and kidneys of the *Plasmodium berghei*-infected mice treated with the samples are presented as photomicrographic images in Fig. 11. Photomicrographs of the kidney sections of the mice (left panel) showed that normal renal corpuscles (black arrows) comprising the Bowman's capsule (white arrow) and the glomerulus (G) were seen in all the groups—groups treated with artemether suspension (sample 21),

artemether-loaded chitosan-coated SRMS-based SLNs (optimized formulation) (sample 2) and unloaded chitosan-modified SRMS-based SLNs (placebo) (sample 23). Furthermore, photomicrographs of the liver sections of the mice (right panel) showed normal plates of hepatocytes (thin black arrows) and central venules (v) in mice group that received the optimized formulation. However, vacuolar degeneration of the hepatocytes and congestion of hepatic central veins were visible in the negative control group (placebo).

Cytotoxicity assay

The cytotoxicity test results for artemether-loaded chitosan-coated SRMS-based SLNs at concentrations

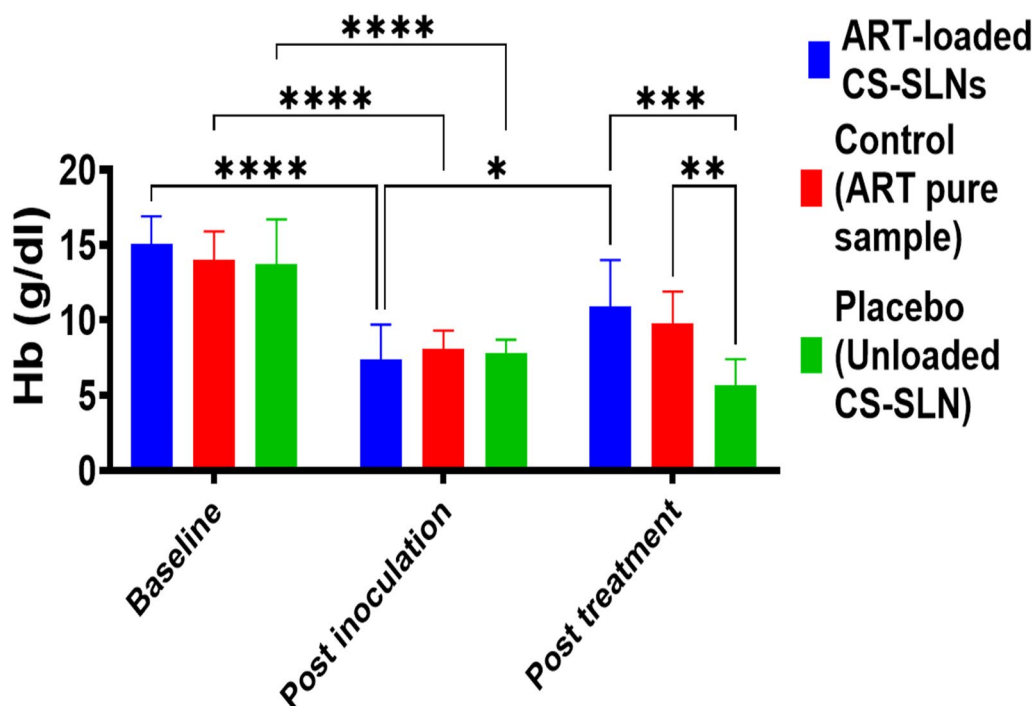


Fig. 9 Hb of mice treated with the formulations. Data were expressed as mean \pm SEM (standard error of mean) $n=6$, differences were considered significant for * $p < 0.05$, ** $p < 0.01$, *** $p < 0.001$ and **** $p < 0.0001$. Key: Post treatment means with peroral treatment, Post inoculation means without peroral treatment, ART pure sample (control) is pure artemether sample, Unloaded CS-SLN is unloaded chitosan-coated SRMS-based SLNs, and ART-loaded CS-SLNs is artemether-loaded chitosan-coated SRMS-based SLNs

0, 25, 50, 100, 200, 300, and 400 $\mu\text{g/ml}$ (presented as in vitro percentage cell viability) are shown in Fig. 12. The untreated control cells did not exhibit any inhibitory effect on the viability of the cells and did not show any detectable cytotoxicity. When compared to the untreated control cells, it was evident that the cell vitality of the plain and artemether-loaded chitosan-coated SLNs was identical, with over 93% cell viability after 24 h at the highest dose utilized in this investigation (400 $\mu\text{g/mL}$).

Stability of the formulations

The results of the stability studies performed on the formulations are shown in Table 4 as well as in Fig. 13. Based on the time-resolved pH-dependent stability study, the pH values were maintained within the acidic region throughout the standard study period, with pH in the range of 5.7–6.0 for plain uncoated SLNs, 5.2–5.5 for plain chitosan-coated SLNs, 6.2–6.5 for artemether-loaded uncoated SLNs and 5.9–6.2 for artemether-loaded chitosan-coated SLNs.

Discussion

The oral bioavailability and poor water solubility of artemether are its defining characteristics. In order to improve the solubility of artemether and promote its intestinal absorption for better treatment of malaria, uncoated SRMS-based SLN and chitosan-coated SRMS-based SLNs were prepared and studied in this work.

Due to the lipophilic nature and low oral bioavailability of artemether, chitosan-decorated SRMS-based SLNs were developed for improved malaria treatment. Screening of the various solid lipid was carried out in this study as an important pre-formulation step in the selection of the best ingredients that would achieve the maximum solubility [47]. Interestingly, C888 and S154 have been employed by our group for the preparation of lipid-based delivery systems containing artemether, with encouraging results [30, 67]. The varying solubility of artemether in these solid lipids could be due to differences in their compositions [55]. According to reports, the high solubilizing capacity of C888 was caused by the existence of mono, di, and triacylglycerols and glycerides of behenic acid [54, 67], while the high solubilizing capacity of S154 was attributed to the amounts of triacylglycerides (94%) and diacylglycerides (6%) [68, 69].

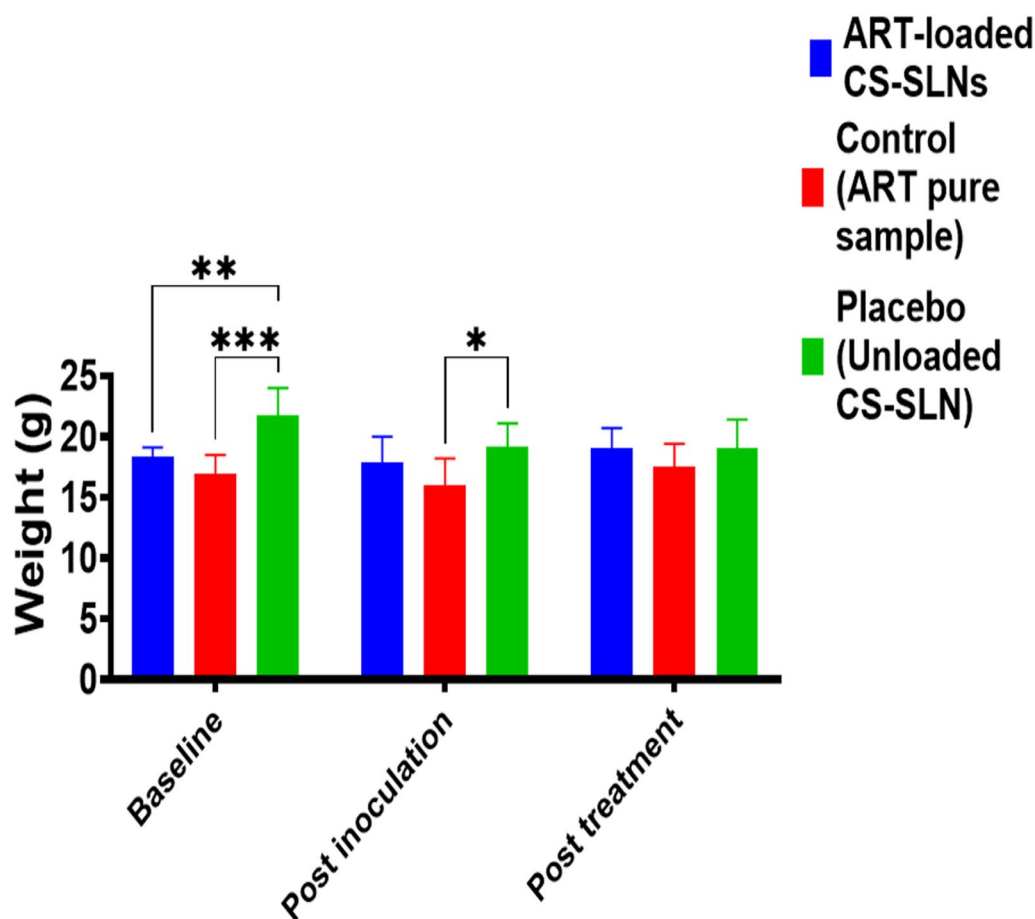


Fig. 10 Weight of mice treated with the formulations. Data were expressed as mean \pm SEM (standard error of mean) $n=6$, differences were considered significant for $*p < 0.05$, $**p < 0.01$ and $***p < 0.001$. Key: Post treatment means with peroral treatment, Post inoculation means without peroral treatment, ART pure sample (control) is pure artemether sample, Unloaded CS-SLN is unloaded chitosan-coated SRMS-based SLNs, and ART-loaded CS-SLNs is artemether-loaded chitosan-coated SRMS-based SLNs

Table 5 Survivability of infected groups of mice (with and without treatment)

Group	Sample code	Treatment	Number of surviving mice post inoculation (before treatment)	Number of surviving mice post treatment	Mortality (%)
I	Y_1	Art-loaded CS-SLNs	6/6	6/6	0.0
II	B	Art pure sample (Control)	6/6	5/6	16.67
II	Y_0	Placebo (Unloaded CS-SLN)	6/6	2/6	66.67

Art Artemether, Y_0 unloaded chitosan-coated SRMS-based SLNs, and Y_1 Artemether-loaded chitosan-coated SRMS-based SLNs

In Table 4, it could be seen that the chitosan coating around the surface of the SLNs contributed to the larger particle sizes compared to uncoated SLNs, which is consistent with previous reports [47–49, 52, 53, 70]. Despite this larger particle size, chitosan-coated SLNs are still within the proper size range for intestinal absorption (< 500 nm), which is relevant to increase the contact with the intestinal mucosa and to facilitate drug permeation [70, 71]. Furthermore, it is discernible

from the results presented in Table 4 that drug incorporation led to a decrease in hydrodynamic diameter, which contradicts previous studies stating that drug incorporation should lead to increase in particle size only [55]. Although the reason for this is not known, it could be associated with other formulation and physicochemical variables. Interestingly, we adopted different strategies in line with established procedures to ensure satisfactory nanoparticle sizes with acceptable PDIs,

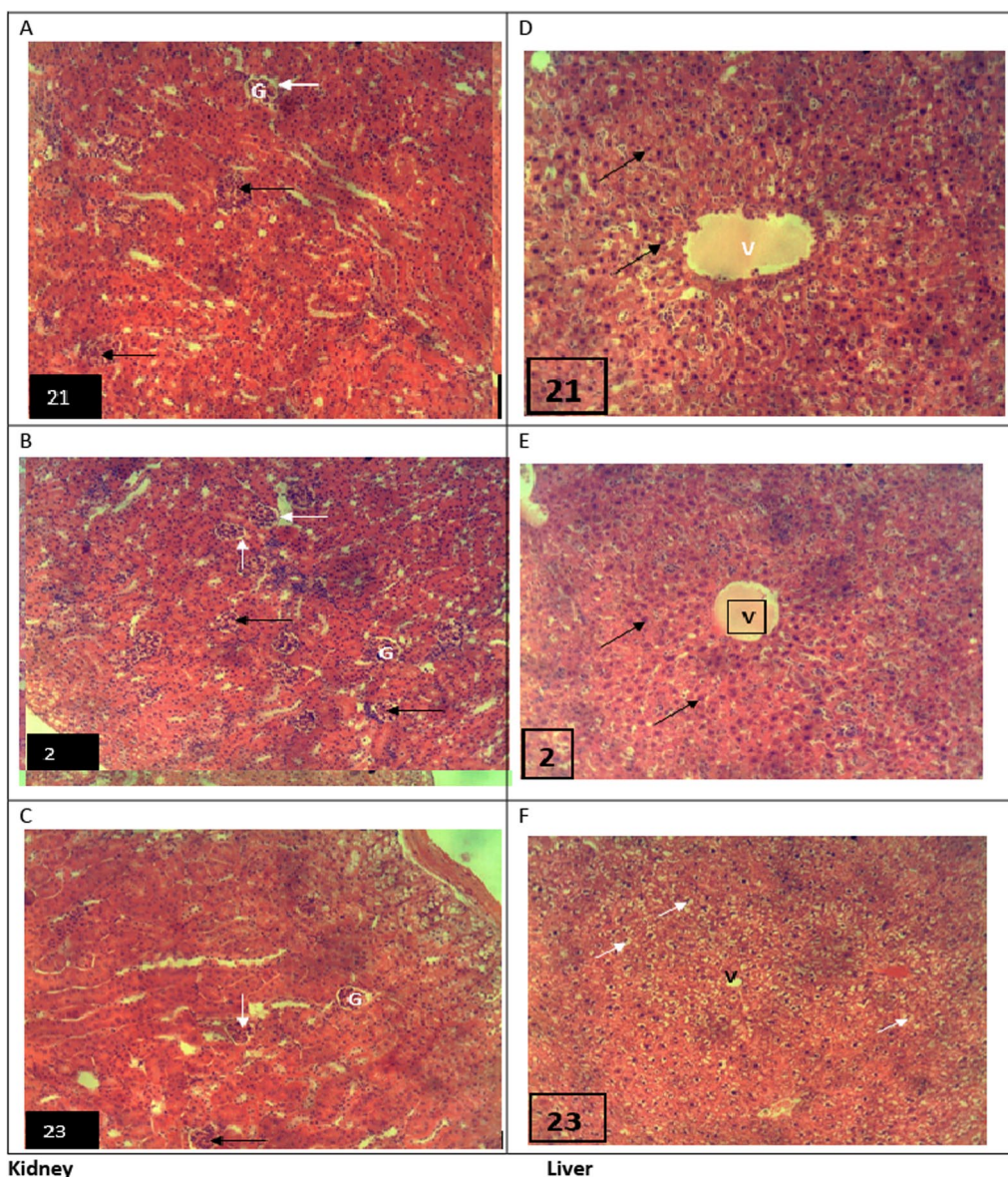


Fig. 11 Histopathological results of **a** artemether suspension (sample 21), **b** artemether-loaded chitosan-coated SRMS-based SLNs (sample 2) and **c** unloaded chitosan-coated SRMS-based SLNs (placebo) (sample 23). Kidney section of mice treated with the formulations containing artemether (**A–C**). Liver section of mice treated with the formulations containing artemether (**D–F**). (H&E 100 \times). Left panel: Photomicrograph of the kidney of rats showing the renal corpuscles (black arrows) comprising the Bowman's capsule (white arrow) and the glomerulus (**G**). Note the myriads of normal renal tubules, surrounding the Bowman's capsules in all the groups. (**H, E** 100 \times). Right panel: Photomicrograph of the liver of mice showing normal plates of hepatocytes (thin black arrows) and central venules (**v**). Note the presence of congested central veins and vacuolar degeneration of the hepatocytes in placebo group. (**H, E** 100 \times)

involving formulation at 10 °C higher than the phase transition temperature of the solid lipids, use of surfactant (Tween[®] 80), incorporation of a stabilizing and solubilizing agent (Soluplus[®]), use of homogenization, utilization of a surface-modifier (P90G) for production of nanosized particles, in line with a recent report by our group [55]. The surface-active agent used in the study reduced the interfacial energy by adsorbing at the

oil–water interface [72], which prevented coalescence of small oil droplets during homogenization [55].

The sample particle size distribution often provides the PDI, a measure of the sample heterogeneity. In this context, a compact size distribution is indicated by a PDI value less than 0.3, values less than 0.5 are within acceptable bounds [43], and values greater than 0.5 imply a broad distribution [73]. On this basis, the PDI

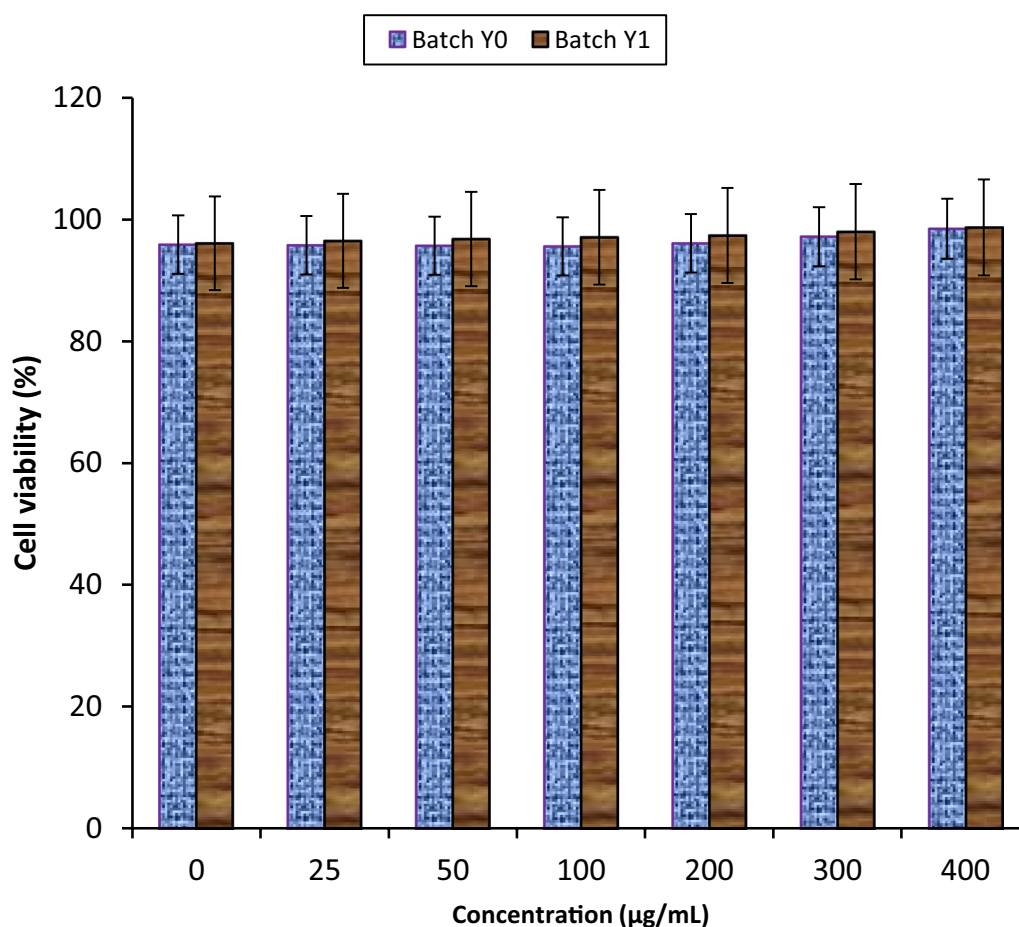


Fig. 12 Cell viability study at different concentrations of optimized artemether-loaded chitosan-coated SLN and unloaded chitosan-coated SLN. Key: Y₀—unloaded chitosan-coated SRMS-based SLNs, and Y₁—artemether-loaded chitosan-coated SRMS-based SLNs. Data are presented as the mean ± standard deviation (n = 3)

values obtained in this study were within the acceptable limits.

The encapsulation of artemether did not alter the surface charge of the nanoparticles, according to the results, but chitosan coating of SLNs significantly ($p < 0.05$) affected their surface charge. Thus, chitosan-coated formulations (batches Y₀ and Y₁) exhibited positive surface charge, providing evidence of chitosan coating. Obviously, plain uncoated SLNs had low zeta potential (-15.55 ± 0.99 mV). Although the exact cause of this is unknown, it is likely due to the presence of non-ionic surfactant and stabilizer (Tween[®] 80 and Soluplus[®]), which is consistent with earlier findings that indicated that non-ionic steric stabilizer adsorption reduced zeta potential by altering the shear plane of the particles in the electrical double layer [74]. Even though such a low zeta potential would have caused agglomeration or aggregation and phase separation in this particular formulation batch, this was not observed in the stability study performed on the

formulations, a situation which could be linked to the steric stabilization effect offered by Soluplus[®]. This goes against previous results [75–77] which stipulated that the zeta potential must be within ± 20 mV for steric stabilization to produce physical stability. Overall, the high zeta-potential values obtained shows that the formulations have good physical stability, due to the electrostatic repulsions between nanoparticles which will prevent SLNs aggregation. Moreover, the positive zeta potential of chitosan-coated formulations resulting from the cationic nature of chitosan will favour interaction between the SLNs and the negatively charged gastrointestinal mucosa and consequently increase the residence time of the SLNs [78].

The solubility of artemether in the lipid matrix (SRMS) of the SLNs and its lipophilic character may be the cause of the elevated EE% and LC observed. The crystalline configuration of solid lipids is disrupted in SLNs, which encourages increased drug loading.

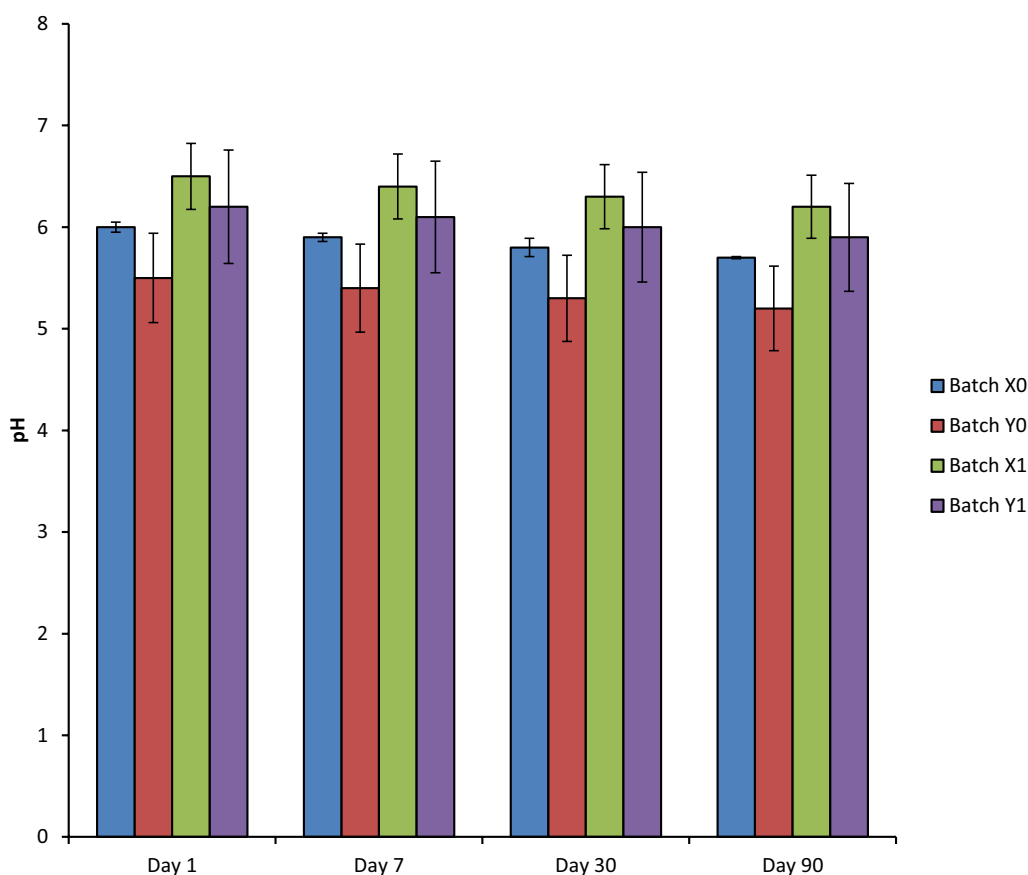


Fig. 13 Time-resolved pH-dependent stability of artemether-loaded chitosan-coated SRMS-based SLNs. Key: X_0 —unloaded uncoated SRMS-based SLNs, Y_0 —unloaded chitosan-coated SRMS-based SLNs, X_1 —artemether-loaded uncoated SRMS-based SLNs and Y_1 —artemether-loaded chitosan-coated SRMS-based SLNs. Data are presented as the mean \pm standard deviation ($n=3$)

Lipids such as C888 which contains mono-, di- and triacylglycerol combinations are capable of encapsulating more drug molecules in the gaps created by the carbon chains [43]. The high EE% observed in this study may reduce the quantity of artemether that is absorbed and reaches the intended site after oral administration. Furthermore, because a high proportion of absorbed drug may pass through the lymphatic transport, high EE% can circumvent the first pass metabolism, a key restriction in oral delivery of artemether [79]. Furthermore, Table 4 revealed that the loading capacity and drug encapsulation efficiency of SLNs were not significantly impacted by the chitosan coating. This result is consistent with earlier research [47–49].

The documented x-ray diffractogram of artemether [23] is compatible with the crystalline structure of artemether, as indicated by the characteristic strong reflections and other reflections of medium and low intensities observed in the diffractogram of artemether. The diffraction pattern of artemether-loaded chitosan-coated SLNs showed that some of the significant peaks of artemether had

disappeared and that the drug's characteristic intensity peaks had decreased, indicating the amorphous state of the drug in the formulation, similar to earlier observation by our group on ciprofloxacin-loaded chitosan-coated SLNs [43]. This suggests that the core of the lipid matrix was effectively used to entrap artemether, enabling controlled drug release. It equally showed that neither did the drug undergo degradation in the developed formulation nor did it crystallize out of the lipid matrix and revealed, in line with earlier results [36, 55, 64], that there was no significant chemical interaction between the drug and the excipients that could predispose to degradation.

The FT-IR spectra of artemether supports the purity of artemether employed in this investigation and is consistent with previously published research on the spectrum of artemether [80]. Identification of the characteristic peaks of artemether in artemether-loaded chitosan-coated SLNs is a strong indication of absence of any incompatibility between the drug and excipients used in the formulation [23, 81]. It could be deciphered from the figures that the peaks in the FT-IR spectrum

of artemether-loaded chitosan-coated SLNs became broader, which may be related to strain, hydrogen bond interactions, or more disorder brought on by a greater temperature [55]. Furthermore, this might possibly be the result of using various materials to prepare artemether-loaded chitosan-coated SRMS-based SLNs [82].

According to the SEM micrographs, the grey structures surrounding the nanoparticles on the surface of the chitosan-coated SLNs indicate the presence of chitosan, which adsorbed on the surface [40–42]. Additionally, the SEM micrograph revealed no drug crystals, indicating effective drug entrapment in the produced SLNs formulations. According to a study published elsewhere [43], the fused nanoparticles seen in the micrographs may have been caused by the sample preparation procedure prior to the analysis.

The release of an unformulated pure sample of artemether was shown to occur more quickly than with SLN formulations, according to data obtained from the release studies. While the burst effect observed with artemether suspension could be attributed to the fact that the drug was not encapsulated in any delivery system, instead of being integrated into the lipid matrix, the untrapped drug may have adsorbed to the surface of the SLNs, causing the burst release of artemether from the formulations [67]. When it comes to delaying the early burst effect and artemether breakdown in the transit zone until it reaches the gut, where absorption occurs, the SLNs showed encouraging and promising potential. Additionally, the release profiles revealed that the chitosan-coated formulation exhibited significantly ($p < 0.05$) lower drug release in comparison to the uncoated one. This suggests that the chitosan coating slowed the release rate and would minimize drug leakage during *in vitro* and *in vivo* delivery [46, 47].

According to earlier research on SLNs, the carrier system could release encapsulated hydrophobic compounds under controlled conditions [74, 79]. In keeping with a previous report on artemether, this was attributed to their solid state at room temperature or body temperature and, in this instance, strong hydrophobic interactions with lipophilic artemether [67]. It was suggested in a different study that the slow diffusion of the drug after being effectively dissolved and encapsulated in the lipid matrix was responsible for the prolonged drug release from SLNs [51–54]. Furthermore, it is possible that the extra barrier provided by the coating layer, which restricts the diffusion of the release medium into the SLNs matrix, is the reason for the lower percentage of artemether released for chitosan-coated SLNs as compared to uncoated formulation [46–54]. It is remarkable and interesting to note that, despite the short half-life of artemether (approximately

three hours following oral administration), the developed artemether-loaded chitosan-coated SLNs (optimized formulation) released the drug over a period of twelve hours, greatly extending the residence time of the drug and permitting a reduction in the frequency of administration [9, 30, 67]. Therefore, *in vivo* pharmacodynamic (antimalarial) experiments were conducted using the optimized formulation, artemether-loaded CS-SLNs, which showed improved and encouraging results in the release study.

In contrast to the negative control, which showed an increase in parasitemia, it was clear from the antimalarial data that the treatments were able to lower the parasitemia levels. Optimized formulation showed better reduction of percent parasitemia than pure artemether which served as the reference (positive control). As a result of its limited water solubility, artemether has a low bioavailability of roughly 40%, which significantly limits its therapeutic potential [9, 23, 29, 30, 58, 67, 80, 81, 83]. Nonetheless, studies have indicated that giving fatty meals to patients enhances the bioavailability of artemether [29, 30]. Our group has severally utilized this idea to enhance oral delivery of artemether using various lipid-based drug delivery systems [9, 30, 36, 61–63, 67, 83].

While it is true that the fatty nanoparticle formulation of artemether may have increased its bioavailability, which would inevitably increase its antimalarial activity, coating the SLNs with chitosan to prepare chitosan-coated SLNs may have prevented degradation of the encapsulated artemether and increased its trans-mucosal permeation or lymphatic transport, in line with previous reports [70, 83]. Inherently, the excipients used in the formulation (Tween[®] 80 serving as surfactant and Soluplus[®] serving as solubilizer or co-surfactant) improved the solubilization of artemether in the matrix core (containing C888 and P90G) and facilitated targeted delivery of the drug to the infected foci of parasitized red blood cells (pRBCs), consistent with several reports by our group [9, 30, 36, 61–64, 67, 83]. Besides, the mucoadhesive cationic biopolymer (chitosan) provided added advantage by increasing the residence time of the nanoparticles in the mucous membrane for a long time sufficient enough to ensure that the malarial parasites are killed [41–49, 70]. This finding is in agreement with the controlled release effect reported in the preceding section regarding *in vitro* release of artemether-loaded chitosan-coated SLNs, which makes the latter a suitable formulation for future application on account of very low parasitemia it recorded in mice. Thus, the outcome of the *in vivo* pharmacodynamic study demonstrated that oral administration of artemether-loaded chitosan-modified SRMS-based SLNs can be employed to treat malaria.

Further pharmacokinetic and biodistribution studies are expected on this optimized formulation.

Regarding the lethality test, the mortality rate of the negative control group must have been influenced by changes in the hematological parameters of the negative control group and the consequent adverse effects, as earlier findings of our group [23, 36] have shown. Whenever mice are infected with *Plasmodium berghei*, they become anemic, which is attributed to erythrocyte destruction, as a result of parasite multiplication or by spleen reticuloendothelial cell action causing the production of phagocytes by the spleen due to abnormal erythrocytes [84, 85]. The anemic condition was obvious in this study because the *P. berghei*-infected mice had decreased PCV and Hb. However, *P. berghei*-induced anemia was vividly reduced in mice that received artemether-loaded formulation which were characterized by increased PCV and Hb levels. Overall results showed that, post-inoculation, the PCV and Hb values decreased in all the groups; however, treatment with optimized formulation and reference (pure artemether sample) increased the PCV and Hb values, whereas there was consistent decrease in the values in the negative control group. Careful assessment of the results showed that the nanosized formulation gave better results than the unformulated drug, that is, there was remarkable alleviation of *P. berghei*-induced anemia by the optimized formulation containing the drug vis-à-vis the pure artemether sample, which could be attributed to the enhanced bioactivity conferred on the drug by the novel delivery system (chitosan-coated SRMS-based SLNs). This outcome is consistent with earlier reports by our group on polymeric and lipid-based antimalarial nanomedicines [9, 23, 36].

The varying weights of the animals show how well the drug is working to address the increasing malaria in the mice, which shows up as an increase in weight (from an increase in the size of the liver, spleen, and probably other blood-forming tissues) [23, 36]. It was obvious that the weight variation was less in the treatment groups in comparison with the negative control group. This finding is in good agreement with our recent reports on polymeric and lipid-based antimalarial nanomedicines [23, 36].

Researchers had earlier suggested that lethality in *Plasmodium berghei*-infected mice could be employed as an indicator for antimalarial efficacy of a drug [9, 86]. In line with earlier findings [9, 86], the fatality of *Plasmodium berghei* infection in infected mice that received unloaded formulation (placebo) was utilized in this investigation as evidence of the virulence of the malarial parasite. It is interesting to note that the strain of *Plasmodium berghei* used in this study is a laboratory model that is frequently used to simulate *Plasmodium falciparum* infection, which causes human malaria [30, 86]. Gladly, the results

obtained from the lethality study corroborated the results obtained in the in vivo antimalarial activity of the samples. As a consequence, the use of the optimized formulation (artemether-loaded chitosan-coated SRMS-based SLNs) in uncomplicated malaria (UM) treatment is warranted and should be initiated.

Kidneys and liver are the major organs implicated in malaria and adverse hepatic and renal histopathological changes are bound to occur in malariogenic mice [9, 23, 65]. The histological findings from the placebo group indicate diseased cells, implying that the signs and symptoms of malaria in the mice group which received the unloaded formulation are still prevalent in this group [2, 9, 65]. A holistic evaluation of the results showed that mice group treated with artemether-loaded chitosan-coated SRMS-based SLNs showed no sign of damage as this optimized formulation exhibited no harmful effects on the liver or kidneys. It is therefore deemed safe for oral administration in these mouse groups. This important observation is consistent with our recent reports on oral polymeric and lipid-based antimalarial nanomedicines [9, 23, 65].

The quantitative percentage response metrics for cell growth inhibition are derived from the drug concentration required to either totally stop cell proliferation or reduce the population by 50% or more [87]. According to the cytotoxicity finding, which is in line with a previous publication [66], the formulations (artemether-loaded and unloaded chitosan-coated SRMS-based SLNs) had no effect on the viability of the cells under the testing conditions. This outcome validates the findings from the histopathology test of the formulations. Interestingly, a recent report on chitosan-coated SLNs did not indicate any form of toxicity, including inhibition of cell viability [42]. Overall, our results, which showed that artemether-loaded chitosan-coated SRMS-based SLNs are not toxic based on the cytotoxicity assessment [88], strongly suggest that these formulations have tremendous potential for in vivo administration as well as for preclinical application.

Obviously, there was insignificant change in pH values of the formulations throughout the study period, an indication that the developed formulations were stable [9]. Regarding particle properties, however, 6 months of storage had no discernible effects on any of the parameters assessed for the formulations, with the exception of the uncoated plain SLNs, which displayed a slight reduction in size that was consistent with previous reports [89–91] and could be attributed to the loss of entrapped solubilized water from the core of the lipid nano- and micro-particulate matrix. Retention of the stability performance by other batches is consistent with our earlier report on chitosan nanoparticles [76]. Given that, in many cases,

chemical and physical instabilities were observed when SLNs were stored as aqueous suspension due to lipid crystallization, polymorphic transformations, aggregation phenomena, and hydrolysis processes [30, 42, 74, 79], this suggests that the developed chitosan-coated SRMS-based SLNs would prevent artemether degradation. This is of great benefit.

Conclusions

This study has demonstrated the first-ever application of SRMS-based chitosan-coated SLNs to boost artemether delivery for better oral malaria therapy. When compared to unformulated artemether (control), the chitosan-coated SLNs protected the drug from GIT degradation, increased its amorphosity, and improved its solubility and dissolution in biorelevant medium. These factors led to enhanced absorption and bioavailability, which in turn accelerated the antimalarial activity of artemether in *Plasmodium berghei*-infected mice. Moreover, the cytotoxicity assessment indicated the safety of the optimized formulation in the GIT region. Having ascertained the good physicochemical performance, safety and efficacy of the developed nano-sized formulation in lower animals, further pharmacokinetic and biodistribution studies should be carried out on the optimized formulation in addition to pilot clinical study in uncomplicated *Plasmodium falciparum* malaria. Efforts should equally be made to ascertain if combination therapy or co-formulation with other antimalarial drugs including second-line and third-line antimalarial drugs as well as with repurposed antimalarials with different mechanisms of action would produce additive or synergistic effect. This will ensure proper utilization of the findings from this study in boosting the malaria armamentarium by developing potential nano-sized artemisinin-based combination therapies, in line with the WHO current recommendations for effective and efficient malaria treatment using ACTs, especially in resource-limited settings.

Abbreviations

SLN	Solid lipid nanoparticles
SRMS	Solidified reverse micellar solution
LC	Loading capacity
EE	Encapsulation efficiency
PDI	Polydispersity index
SA	Stearic acid
S154	Softisan® 154
C888	Compritol® 888 ATO
SEM	Scanning electron microscopy
FT-IR	Fourier transform infra-red
ATR-FTIR	Attenuated total reflectance- Fourier transform infrared
PXRD	Powder x-ray diffraction
WHO	World Health Organization
GIT	Gastrointestinal tract
PBS	Phosphate buffered saline
P90G	Phospholipon® 90G
UCH	University College Hospital
PSU	Prince of Songkla University

pRBC	Parasitized red blood cells
G	Glomerulus
H & E	Hematoxylin and eosin
CS	Chitosan
CS-SLN	Chitosan-coated solid lipid nanoparticles
UM	Uncomplicated malaria
ACTs	Artemisinin-based combination therapies
Hb	Hemoglobin
PCV	Packed cell volume
RBC	Red blood cells
Pb	<i>Plasmodium berghei</i>
CPb	Chloroquine-sensitive <i>Plasmodium berghei</i>
DMSO	Dimethylsulphoxide
Art	Artemether
X ₀	Unloaded uncoated solidified reverse micellar solution-based solid lipid nanoparticles
Y ₀	Unloaded chitosan-coated solidified reverse micellar solution-based solid lipid nanoparticles
X ₁	Artemether-loaded uncoated solidified reverse micellar solution-based solid lipid nanoparticles
Y ₁	Artemether-loaded chitosan-coated solidified reverse micellar solution-based solid lipid nanoparticles

Supplementary Information

The online version contains supplementary material available at <https://doi.org/10.1186/s13065-025-01422-4>.

Supplementary material 1

Acknowledgements

We thank Phospholipid GmbH, Koln, Germany for kind provision of Phospholipon® 90G used in this study as well as May and Baker PLC, Ikeja, Lagos, Nigeria, for the kind gift of pure artemether sample.

Author contributions

FCK conceptualized, designed, supervised, and drafted the manuscript and participated in funding acquisition. KCU participated in drafting the manuscript. CSO prepared drug stock solutions. MEO prepared part of the introduction. THG participated in characterization of the formulations. REE performed weight determination. CPA prepared part of the introduction and participated in funding acquisition. MAM participated in the investigation, in funding acquisition and in revising the manuscript. AIO participated in the safety studies. CSN performed the stability studies. OLU participated in release experiments. ECO participated in hematological studies. CEU participated in release studies. PAA performed the data analysis. ACE participated in lethality studies. SWU performed UV analysis. COU was involved in FT-IR spectroscopic analysis. WIU performed the antimalarial and histological evaluations and participated in funding acquisition. ST participated in characterization of the formulations and in revising the manuscript. AAA provided some excipients used in the study, participated in funding acquisition and in revising the manuscript. All authors read, reviewed and approved the final manuscript.

Funding

This research work received financial support from Tertiary Education Trust Fund (TETFund) (Grant No. TETFUND/DR&D/CE/NRF/2019/STI/46/) by Government of Nigeria. Prof. Franklin Chimaobi Kenechukwu is the principal investigator and recipient of the grant.

Availability of data and materials

All data generated or analyzed during this study are included in this published article.

Declarations

Ethics approval and consent to participate

The animal experimental protocols were in accordance with the guidelines for conducting animal experiments and were approved by the University of Nigeria, Nsukka Animal Ethics Committee (Faculty of Pharmaceutical Sciences

Research Ethics, approval number FPSRE/UNN/20/00064) and in compliance with the Federation of European Laboratory Animal Science Association and the European Union Directive 2010/63/EU for animal experiments.

Consent for publication

Not applicable. This work does not contain data from any individual person.

Competing interests

The authors declare no competing interests.

Author details

¹Drug Delivery and Nanomedicines Research Laboratory, Department of Pharmaceutics, Faculty of Pharmaceutical Sciences, University of Nigeria, Nsukka 410001, Enugu State, Nigeria. ²Department of Pharmaceutical Microbiology and Biotechnology, Faculty of Pharmaceutical Sciences, University of Nigeria, Nsukka 410001, Enugu State, Nigeria. ³Department of Pharmaceutical Microbiology and Biotechnology, Faculty of Pharmaceutical Sciences, David Umahi Federal, University of Health Sciences, Uburu, Ebonyi State, Nigeria. ⁴Department of Pharmaceutical Technology and Industrial Pharmacy, Faculty of Pharmaceutical Sciences, University of Nigeria, Nsukka 410001, Enugu State, Nigeria. ⁵Department of Biochemistry, Faculty of Biological Sciences, University of Nigeria, Nsukka 410001, Enugu State, Nigeria. ⁶Nanomedicines Unit, NANOMED, Universidade Federal Do ABC Santo Andre, Sao Paulo, Brazil. ⁷Department of Science Laboratory Technology, Faculty of Physical Sciences, University of Nigeria, Nsukka 410001, Enugu State, Nigeria. ⁸Department of Veterinary Anatomy and Microbiology, Faculty of Veterinary Medicine, University of Nigeria, Nsukka 410001, Enugu State, Nigeria. ⁹Drug Delivery System Excellence Center (DDSEC), Department of Pharmaceutical Technology, Faculty of Pharmaceutical Sciences, Prince of Songkla University, Hat Yai 90110, Songkhla, Thailand.

Received: 4 July 2024 Accepted: 14 February 2025

Published online: 08 March 2025

References

- Talapak J, Škrlec I, Alebić T, Jukić M, Včev A. Malaria: the past and the present. *Microorganisms*. 2019;7(6):179. <https://doi.org/10.3390/microorganisms7060179>.
- Uzundu S, Echezona A, Nwagwu C, Onugwu A, Ugorji L, Agbo C, Kenechukwu F, Ogbonna J, Akpa P, Nnamani P, Momoh A, Attama A. Combating antimalarial drug resistance: Recent advances and future perspectives. In: Piccaluga PP, editor. *Malaria*. London: IntechOpen; 2022. Fact sheet about malaria. <https://www.who.int/news-room/fact-sheets/detail/malaria>. Accessed 21 Apr 2024.
- Prado GRL, Garcia CH, Cea LM, et al. Malaria in developing countries. *J Infect Dev Ctries*. 2014;8(01):001–4. <https://doi.org/10.3855/jidc.4610>.
- World Health Organization (WHO) guidelines for malaria - 16 October 2023. <https://app.magicapp.org/#/guideline/LwRMXj/section/j7DB3L>. Accessed 21 Apr 2024.
- Agbo CP, Ugwuanyi TC, Eze OC, Onugwu LA, Echezona AC, Nwagwu SC, Uzundu S, Ogbonna JDN, Ugorji OL, Nnamani PO, Akpa PA, Reginald-Opara JN, Mcconville C, Attama AA, Ofokansi KC. Quinine: Redesign and rerouted. *Processes*. 2023;11(1):1–21. <https://doi.org/10.3390/pr11061811>.
- Ocan M, Nakalembe L, Otike C, Omali D, Buzibye A, Nsohya S. Pharmacopeial quality of artemether – lumefantrine anti-malarial agents in Uganda. *Malar J*. 2023;22(165):1–11. <https://doi.org/10.1186/s12936-023-04600-8>.
- Cowman AF, Healer J, Marapana D, Marsh K. Malaria: biology and disease. *Cell*. 2016;167(3):610–24. <https://doi.org/10.1016/j.cell.2016.07.055>.
- Akpa PA, Ugwuoke JA, Attama AA, Ugwu CN, Ezeibe EN, Momoh MA, Echezona AC, Kenechukwu FC. Improved antimalarial activity of caprol-based nanostructured lipid carriers encapsulating artemether-lumefantrine for oral administration. *Afr Health Sci*. 2020;20(4):1679–97. <https://doi.org/10.4314/ahs.v20i4.20>.
- Patel CA, Pande S, Shukla P, Ranch K, Al-Tabakha MM, Boddu SHS. Antimalarial drug resistance: trends, mechanisms, and strategies to combat antimalarial resistance. In: Shegokar R, Pathak Y, editors. *Malarial drug delivery systems: advances in treatment of infectious diseases*. Cham: Springer International Publishing; 2023. p. 43–69.
- Ravindar L, Hasbullah SA, Rakesh KP, Raheem S, Agustar HK, Ismail N, Ling LY, Hassan NI. Exploring diverse frontiers: advancements of bioactive 4-aminoquinoline-based molecular hybrids in targeted therapeutics and beyond. *Eur J Med Chem*. 2024;264:116043. <https://doi.org/10.1016/j.ejmech.2023.116043>.
- Ravindar L, Hasbullah SA, Rakesh KP, Hassan NI. Recent developments in antimalarial activities of 4-aminoquinoline derivatives. *Eur J Med Chem*. 2023;256:115458. <https://doi.org/10.1016/j.ejmech.2023.115458>.
- Ravindar L, Hasbullah SA, Rakesh KP, Hassan NI. Triazole hybrid compounds: a new frontier in malaria treatment. *Eur J Med Chem*. 2023;259:115694. <https://doi.org/10.1016/j.ejmech.2023.115694>.
- Ravindar L, Hasbullah SA, Rakesh KP, Hassan NI. Pyrazole and pyrazoline derivatives as antimalarial agents: a key review. *Eur J Pharm Sci*. 2023;183:106365. <https://doi.org/10.1016/j.ejps.2022.106365>.
- Zha G-F, Rakesh KP, Manukumar HM, Shantharam CS, Long S. Pharmaceutical significance of azepane based motifs for drug discovery: a critical review. *Eur J Med Chem*. 2019;162:465–94. <https://doi.org/10.1016/j.ejmech.2018.11.031>.
- Rakesh KP, Shantharam CS, Sridhara MB, Manukumar HM, Qin H-L. Benzisoxazole: a privileged scaffold for medicinal chemistry. *Med Chem Commun*. 2017;8:2023–39. <https://doi.org/10.1039/C7MD00449D>.
- Qin H-L, Zhang Z-W, Ravindar L, Alsulami H, Rakesh KP. Chalcone hybrids as privileged scaffolds in antimalarial drug discovery: a key review. *Eur J Med Chem*. 2020;2020(193):112215. <https://doi.org/10.1016/j.ejmech.2020.112215>.
- Fang W-Y, Ravindar L, Rakesh KP, Manukumar HM, Shantharam CS, Alharbi NS, Qin H-L. Synthetic approaches and pharmaceutical applications of chloro-containing molecules for drug discovery: a critical review. *Eur J Med Chem*. 2019;173:117–53. <https://doi.org/10.1016/j.ejmech.2019.03.063>.
- Zhao C, Rakesh KP, Ravindar L, Fang W-Y, Qin H-L. Pharmaceutical and medicinal significance of sulfur (S^{VI})-Containing motifs for drug discovery: a critical review. *Eur J Med Chem*. 2019;162:679–734. <https://doi.org/10.1016/j.ejmech.2018.11.017>.
- Dong P, Rakesh KP, Manukumar HM, Mohammed YHE, Karthik CS, Sumathi S, Mallu P, Qin H-L. Innovative nano-carriers in anticancer drug delivery—a comprehensive review. *Bioorg Chem*. 2019;85:325–36. <https://doi.org/10.1016/j.bioorg.2019.01.019>.
- Tsheha ST. *Plasmodium* species and drug resistance. In: Tyagi RK, editor. *Plasmodium species and drug resistance*. London: IntechOpen; 2021.
- Maiga FO, Wele M, Toure SM, et al. Artemisinin-based combination therapy for uncomplicated *Plasmodium falciparum* malaria in Mali: a systematic review and meta-analysis. *Malar J*. 2021;20(1):356. <https://doi.org/10.1186/s12936-021-03890-0>.
- Kenechukwu FC, Dias ML, Neto RPC, Ricci-Júnior E. Compatibilized biopolymer-based core-shell nanoparticles: a new frontier in malaria combo-therapy. *J Pharm Innov*. 2023;18(2):594–620. <https://doi.org/10.1007/s12247-022-09664-8>.
- Kamchonwongpaisan S, Meshnick SR. The mode of action of the antimalarial artemisinin and its derivatives. *Gen Pharm Vasc Syst*. 1996;27:587–92.
- Meshnick SR. Artemisinin: mechanism of action, resistance and toxicity. *Int J Parasitol*. 2002;32:1655–60.
- Meshnick SR, Taylor TE, Kamchonwongpaisan S. Artemisinin and the antimalarial endoperoxides: from herbal remedy to targeted chemotherapy. *Microbiol Rev*. 1996;60:301–15.
- Muller IB, Hyde JB. Antimalarial drugs: modes of action and mechanisms of parasite resistance. *Future Microbiol*. 2010;5:1–7.
- Faurant C. From bark to weed: the history of artemisinin. *Parasite*. 2011;18(3):215–8. <https://doi.org/10.1051/parasite/2011183215>.
- Momoh MA, Kenechukwu FC, Ugwu CE, Adedokun MO, Agboke AA, Agbo CP, Ossai EC, Ofomata AC, Youngson DC, Omeje CE, Amadi BC. Development and evaluation of artemether-loaded microspheres delivery system for oral application in malaria treatment. *Trop J Nat Prod Res*. 2021;5(11):2030–6.
- Agbo CP, Umeyor CE, Kenechukwu FC, Ogbonna JDN, Chime SA, Charles L, Agubata CO, Ofokansi KC, Attama AA. Formulation design, in vitro characterizations and anti-malarial investigations of artemether and lumefantrine-entrapped solid lipid microparticles. *Drug Dev Ind Pharm*. 2016;42(10):1708–21. <https://doi.org/10.3109/03639045.2016.1171331>.

31. Kenechukwu FC, Momoh MA, Nnamani PO, Attama AA. Solid lipid micro-dispersions (SLMs) based on PEGylated solidified reverse micellar solutions (SRMS): a novel carrier system for gentamicin. *Drug Deliv*. 2015;22(6):710–22. <https://doi.org/10.3109/10717544.2014.900152>.
32. Kenechukwu FC, Isaac GT, Nnamani DO, Momoh MA, Attama AA. Enhanced circulation longevity and pharmacodynamics of metformin from surface-modified nanostructured lipid carriers based on solidified reverse micellar solutions. *Heliyon*. 2022;8(3):e09100. <https://doi.org/10.1016/j.heliyon.2022.e09100>.
33. Chime SA, Attama AA, Kenechukwu FC, Umeyor CE, Onunkwo GC. Formulation, in vitro and in vivo characterisation of diclofenac potassium sustained release tablets based on solidified reverse micellar solution (SRMS). *Br J Pharm Res*. 2013;3(1):90–107. <https://doi.org/10.9734/bjpr/2014/1567>.
34. Nanjwade BK, Patel DJ, Udhani RA, Manvi FV. Functions of lipids for enhancement of oral bioavailability of poorly water-soluble drugs. *Sci Pharm*. 2011;79:705–27. <https://doi.org/10.3797/scipharm.1105-09>.
35. Dahan A, Hoffman A. Rationalizing the selection of oral lipid based drug delivery systems by an in vitro dynamic lipolysis model for improved oral bioavailability of poorly water soluble drugs. *J Control Rel*. 2008;129(1):1–10. <https://doi.org/10.1016/j.jconrel.2008.03021>.
36. Attama AA, Kenechukwu FC, Onuigbo EB, Nnamani PO, Obitte NC, Finke JH, Pretor S, Muller-Goymann CC. Solid lipid nanoparticles encapsulating a fluorescent marker (coumarin 6) and anti-malarials – artemether and lumefantrine: evaluation of cellular uptake and anti-malarial activity. *Eur J Nanomed*. 2016;8(3):129–38.
37. Kenechukwu FC, Nnamani DO, Duhu JC, Nmesirionye BU, Momoh MA, Akpa PA, Attama AA. Potential enhancement of metformin hydrochloride in solidified reverse micellar solution-based PEGylated lipid nanoparticles targeting therapeutic efficacy in diabetes treatment. *Heliyon*. 2022;8:e09099. <https://doi.org/10.1016/j.heliyon.2022.e09099>.
38. Kenechukwu FC, Attama AA, Ibezim EC, Nnamani PO, Umeyor CE, Uronnachi EM, Momoh MA, Akpa PA. Tailor-made mucoadhesive lipid nanogel improves oromucosal antimycotic activity of encapsulated miconazole nitrate. *Eur J Nanomed*. 2017;9(3–4):115–26. <https://doi.org/10.1515/ejnm-2017-0010>.
39. Kenechukwu FC, Attama AA, Ibezim EC. Novel solidified reverse micellar solution-based mucoadhesive nano lipid gels encapsulating miconazole nitrate-loaded nanoparticles for improved treatment of oropharyngeal candidiasis. *J Microencapsul*. 2017;34(6):592–609. <https://doi.org/10.1080/02652048.2017.1370029>.
40. Sohaib M, Shah SU, Shah KU, Khan NR, Irfan MM, Niazi ZR, Alqahtani AA, Alasiri A, Walbi IA, Mahmood S. Physicochemical characterization of chitosan-decorated finasteride solid lipid nanoparticles for skin drug delivery. *BioMed Res Int*. 2022;2012:1–10. <https://doi.org/10.1155/2022/7792180>.
41. Shi L, Lu J, Cao Y, Liu J-Y, Zhang X-X, Zhang H, Cui J-H, Cao Q-R. Gastrointestinal stability, physicochemical characterization and oral bioavailability of chitosan or its derivatives-modified solid lipid nanoparticles loading docetaxel. *Drug Dev Ind Pharm*. 2016. <https://doi.org/10.1080/03639045.2016.1220571>.
42. Piazzini V, Cinci L, D'Ambrosio M, Luceri C, Bergonzi Biliaa AR, MC. Solid lipid nanoparticles and chitosan-coated solid lipid nanoparticles as promising tool for silybin delivery: formulation, characterization, and in vitro evaluation. *Current Drug Deliv*. 2019;16:142–52.
43. Onugwu LA, Attama AA, Nnamani PO, Onugwu SO, Onuigbo EB, Khutorvanskiy VV. Development and optimization of solid lipid nanoparticles coated with chitosan and poly(2-ethyl-2-oxazoline) for ocular drug delivery of ciprofloxacin. *J Drug Deliv Sci Technol*. 2022. <https://doi.org/10.1016/j.jddst.2022.103527>.
44. Nagpal K, Singh SK, Mishra DN. Chitosan nanoparticles: a promising system in novel drug delivery. *Chem Pharm Bull*. 2010;58(11):1423–30.
45. Wang Y, Li P, Kong L. Chitosan-modified PLGA nanoparticles with versatile surface for improved drug delivery. *AAPS PharmSciTech*. 2013;14(2):585–92. <https://doi.org/10.1208/s12249-013-9943-3>.
46. Wang JJ, et al. Recent advances of chitosan nanoparticles as drug carriers. *Int J Nanomed*. 2011;6:765–74. <https://doi.org/10.2147/ijn.s17296>.
47. Hassan DM, El-Kamel AH, Allam EA, Bakr BA, Ashour AA. Chitosan-coated nanostructured lipid carriers for effective brain delivery of Tanshinone IIA in Parkinson's disease: interplay between nuclear factor-kappa β and cathepsin B. *Drug Deliv Transl Res*. 2023. <https://doi.org/10.1007/s13346-023-01407-7>.
48. Raj R, Wairkar S, Sridhar V, Gaud R. Pramipexole dihydrochloride loaded chitosan nanoparticles for nose to brain delivery: development, characterization and in vivo anti-parkinson activity. *Int J Biol Macromol*. 2018;109:27–35.
49. Gartzandia O, Herrán E, Ruiz-Ortega JA, Miguez C, Igartua M, Lafuente JV, et al. Intranasal administration of chitosan-coated nanostructured lipid carriers loaded with GDNF improves behavioral and histological recovery in a partial lesion model of parkinson's disease. *J Biomed Nanotechnol*. 2016;12:2220–30.
50. Manigandan V, Nataraj J, Karthik R, Manivasagam T, Saravanan R, Thenmozhi AJ, et al. Low molecular weight sulfated chitosan: neuroprotective effect on rotenone-induced *in vitro* parkinson's disease. *Neurotox Res*. 2019;35:505–15.
51. Sardoiwala MN, Karmakar S, Choudhury SR. Chitosan nanocarrier for FTY720 enhanced delivery retards parkinson's disease via PP2A-EzH2 signaling in vitro and ex vivo. *Carbohydr Polym*. 2021;254:117435.
52. Pyo YC, Tran P, Kim DH, Park JS. Chitosan-coated nanostructured lipid carriers of fenofibrate with enhanced oral bioavailability and efficacy. *Colloids Surf B Biointerf*. 2020;196:111331.
53. Gartzandia O, Herran E, Pedraz JL, Carro E, Igartua M, Hernandez RM. Chitosan coated nanostructured lipid carriers for brain delivery of proteins by intranasal administration. *Colloids Surf B Biointerf*. 2015;134:304–13.
54. Shah B, Khunt D, Bhatt H, Misra M, Padh H. Application of quality by design approach for intranasal delivery of rivastigmine loaded solid lipid nanoparticles: effect on formulation and characterization parameters. *Eur J Pharm Sci*. 2015;78:54–66. <https://doi.org/10.1016/j.ejps.2015.07.002>.
55. Agbo CP, Ugwuanyi TC, Ugwuoke WI, McConville C, Attama AA, Ofokansi KC. Intranasal artesunate-loaded nanostructured lipid carriers: a convenient alternative to parenteral formulations for the treatment of severe and cerebral malaria. *J Control Rel*. 2021;334:224–36. <https://doi.org/10.1016/j.jconrel.2021.04.020>.
56. Kenechukwu FC, Nnamani DO, Nmesirionye BU, Isaac GT, Momoh MA, Attama AA. PEGylated lipid nanocontainers tailored with sunseed-oil-based solidified reverse micellar solution for enhanced pharmacodynamics and pharmacokinetics of metformin. *J Pharm Innov*. 2022. <https://doi.org/10.1007/s12247-022-09654-w>.
57. Kenechukwu FC, Attama AA, Ibezim EC, Nnamani PO, Umeyor CE, Uronnachi EM, Gugu TH, Momoh MA, Ofokansi KC, Akpa PA. Surface-modified mucoadhesive microgels as a controlled release system for miconazole nitrate to improve localized treatment of vulvovaginal candidiasis. *Eur J Pharm Sci*. 2018;111:358–75. <https://doi.org/10.1016/j.ejps.2017.10.002>.
58. Jain K, Sood S, Gowthamarajan K. Optimization of artemether-loaded NLC for intranasal delivery using central composite design. *Drug Deliv*. 2015. <https://doi.org/10.3109/10717544.2014.885999>.
59. Kenechukwu FC, Kalu CF, Momoh MA, Onah AI, Attama AA, Okore VC. Novel *Bos indicus* fat-based nanoparticle lipospheres of miconazole nitrate as enhanced mucoadhesive therapy for oral candidiasis. *BioInterv Res Appl Chem*. 2023;13(24):1–19. <https://doi.org/10.33263/BRIC131.024>.
60. Borhade V, Pathak S, Sharma S, Patravale V. Clotrimazole nanoemulsion for malaria chemotherapy. Part II: stability assessment, in vivo pharmacodynamic evaluations and toxicological studies. *Int J Pharm*. 2012;431(1–2):149–60. <https://doi.org/10.1016/j.ijpharm.2011.12.031>.
61. Nnamani PO, Ugwu AA, Nnadi OH, Kenechukwu FC, Ofokansi KC, Attama AA, Lehr C-M. Formulation and evaluation of transdermal nanogel for delivery of artemether. *Drug Deliv Transl Res*. 2021;11(4):1655–74. <https://doi.org/10.1007/s13346-021-00951-4>.
62. Nnamani PO, Ugwu AA, Ibezim EC, Kenechukwu FC, Akpa PA, Ogbonna JDN, Obitte NC, Odo AN, Windbergs M, Lehr CM, Attama AA. Sustained-release liquisolid compact tablets containing artemether-lumefantrine as alternate-day regimen for malaria treatment to improve patient compliance. *Int J Nanomed*. 2016;11:6365–78.
63. Ogbonna JDN, Echezona AC, Nwagwu CS, Agbo CP, Onugwu AL, Kenechukwu FC, Akpa PA, Momoh MA, Attama AA. Formulation, *in vitro* and *in vivo* evaluation of sustained released artemether-lumefantrine-loaded microstructured solid lipid microparticles (SLMs). *Trop J Nat Prod Res*. 2021;5(8):1460–9. <https://doi.org/10.26538/tjnp/v5i8.23>.
64. Umeyor CE, Okoye I, Uronnachi EM, Okeke T, Kenechukwu FC, Attama AA. Repositioning miconazole nitrate for malaria: Formulation of sustained

- release nanostructured lipid carriers, structure characterization and *in vivo* antimalarial evaluation. *J Drug Deliv Sci Tech.* 2021;61:102125. <https://doi.org/10.1016/j.jddst.2020.102125>.
65. Ogbonna JDN, Nzekwe IT, Kenechukwu FC, Nwobi CS, Amah JI, Attama AA. Development and evaluation of chloroquine phosphate microparticles using solid lipid as a delivery carrier. *J Drug Discov Dev Deliv.* 2015;2(1):1011.
 66. Momoh MA, Kenechukwu FC, Ofokansi KC, Attama AA, Díaz DD. Insulin-loaded mucoadhesive nanoparticles based on mucin-chitosan complexes for oral delivery and diabetes treatment. *Carbohydr Polym.* 2020;229:115506. <https://doi.org/10.1016/j.carbpol.2019.115506>.
 67. Nnamani PO, Kenechukwu FC, Nwagwu SC, Okoye O, Attama AA. Physicochemical characterization of artemether-entrapped solid lipid microparticles prepared from templated-compritol and *Capra hircus* (goat fat) homolipid. *Dhaka Univ J Pharm Sci.* 2021;20(1):67–80. <https://doi.org/10.3329/dujps.v20i1.54034>.
 68. Efendy GD, Sheikh AKSH, Latip NA, Rahim SA, Mazlan M. Palm oil in lipid-based formulations and drug delivery systems. *Biomolecules.* 2019;9:64.
 69. Umevor CE, Kenechukwu FC, Ogbonna JDN, Chime SA, Attama AA. Preparation of novel solid lipid microparticles loaded with gentamicin and its evaluation *in vitro* and *in vivo*. *J Microencapsul.* 2012;29(3):296–307.
 70. Fonte P, Nogueira T, Gehm C, Ferreira D, Sarmento B. Chitosan-coated solid lipid nanoparticles enhance the oral absorption of insulin. *Drug Deliv Transl Res.* 2011;1:299–308.
 71. Florence AT. Issues in oral nanoparticle drug carrier uptake and targeting. *J Drug Target.* 2004;12:65–70.
 72. Chime SA, Kenechukwu FC, Attama AA. Nanoemulsions- advances in formulation, characterization and applications in drug delivery. In: Salcido A, editor. *Application of nanotechnology in drug delivery.* London: INTECH Publishers; 2014. p. 77–126.
 73. Hoseini B, Jaafari M, Golabpour A, Momtazi-Borojeni A, Karimi M, Eslami S. Application of ensemble machine learning approach to assess the factors affecting size and polydispersity index of liposomal nanoparticles. *Sci Rep.* 2023;13(1):18012.
 74. Ozdemir S, Çelik B, Üner M. Properties and therapeutic potential of solid lipid nanoparticles and nanostructured lipid carriers as promising colloidal drug delivery systems. *Mater Biomed Eng.* 2019. <https://doi.org/10.1016/b978-0-12-816913-1.00015-5>.
 75. Tamjidi F, Shahedi M, Varshosaz J, Nasirpour A. Nanostructured lipid carriers (NLC): a potential delivery system for bioactive food molecules. *Innov Food Sci Emerg Technol.* 2013;19:29–43. <https://doi.org/10.1016/J.JFSET.2013.03.002>.
 76. Lakshmi P, Kumar GA. Nanosuspension technology: a review. *Int J Pharm Pharm Sci.* 2010;2:35–40.
 77. Mitri K, Shegokar R, Gohla S, Anselmi C, Müller RH. Lipid nanocarriers for dermal delivery of lutein: preparation, characterization, stability and performance. *Int J Pharm.* 2011;414:267–75.
 78. Wang F, Zhang M, Zhang D, Huang Y, Chen L, Jiang S, Shi K, Li R. Preparation, optimization, and characterization of chitosan coated solid lipid nanoparticles for ocular drug delivery. *J Biomed Res.* 2018;32:411–23.
 79. Venishetty VK, Chede R, Komuravelli R, Adepu L, Sistla R, Diwan PV. Design and evaluation of polymer coated carvedilol loaded solid lipid nanoparticles to improve the oral bioavailability: a novel strategy to avoid intraduodenal administration. *Colloids Surf B Biointerfaces.* 2012;95:1–9.
 80. Yahaya ZS, Ofokansi KC, Allagh ST, Bhatia PG. Preparation and characterization of artemether inclusion complexes with hydroxypropyl- β -cyclodextrin. *Trop J Pharm Res.* 2017;16:2359–64.
 81. Awofisayo SO, Arhewoh M, Okhamafe AO. *In vitro* interaction studies between artemether – lumefantrine and lamivudine/metronidazole. *Int J Curr Res Rev.* 2018;10:25–30.
 82. Umit G, Ike U, Gulgun Y, Fatma KE, Aydogmus Z. Formulation and characterization of solid lipid nanoparticles, nanostructured lipid carriers and nanoemulsion of lornoxicam for transdermal delivery. *Acta Pharma.* 2015;65:1–13. <https://doi.org/10.1515/acph-2015-0009>.
 83. Agubata CO, Nzekwe IT, Attama AA, Mueller-Goymann CC, Onunkwo GC. Formulation, characterization and anti-malarial activity of homolipid-based artemether microparticles. *Int J Pharm.* 2015;478:202–22.
 84. Lefèvre G, Thomsen MS. Clinical pharmacokinetics of artemether and lumefantrine (Riamet®). *Clin Drug Investig.* 1999;18:467–80.
 85. Nardos A, Makonnen E. *In vivo* antiplasmodial activity and toxicological assessment of hydroethanolic crude extract of *Ajuga remota*. *Malaria J.* 2017;16(25):1–8.
 86. Adeyemi OI, Ige OO, Akanmu MA, Ukponmwan OE. *In vivo* anti-malarial activity of propranolol against *Plasmodium berghei* ANKA infection in mice. *Afr J Exper Microbiol.* 2020;21(4):333–9.
 87. Heiser LM, Sadanandam A, Kuo W-L, Benz SC, Goldstein TC, Ng S, et al. Subtype and pathway specific responses to anticancer compounds in breast cancer. *Proc Natl Acad Sci.* 2012;109:2724–9.
 88. Dibua EU, Okeke CC, Ugwu C, Kenechukwu FC, Okorie A. *In vivo* anti-malarial and cytotoxicity activity of ethanolic stem bark of *Petersianthus macrocarpus* and leaf of *Astonia boonei* in experimental mice model. *Int J Curr Microbiol Appl Sci.* 2013;2(12):354–68.
 89. Radomska-Soukharev A, Muller RH. Chemical stability of lipid excipients in SLN: production of test formulations, characterization and short-term stability. *Pharmazie.* 2006;61:425–30.
 90. Cirri M, Mennini N, Maestrelli F, Mura P, Ghelardini C, Mannelli LDC. Development and *in vivo* evaluation of an innovative “hydrochlorothiazide-in cyclodextrins-in solid lipid nanoparticles” formulation with sustained release and enhanced oral bioavailability for potential hypertension treatment in pediatrics. *Int J Pharm.* 2017;521:73–83.
 91. Momoh MA, Adedokun MO, Adikwu MU, Ibezim EC. *In vitro* evaluation of PEGylated-mucin matrix as carrier for oral delivery of metformin hydrochloride. *Trop J Pharm Res.* 2014;13(7):1039–45. <https://doi.org/10.4314/tjpr.v13i7.5>.

Publisher's Note

Springer Nature remains neutral with regard to jurisdictional claims in published maps and institutional affiliations.